iScience

CellPress
OPEN ACCESS

Article

Oxygen tension-dependent variability in the cancer cell kinome impacts signaling pathways and response to targeted therapies

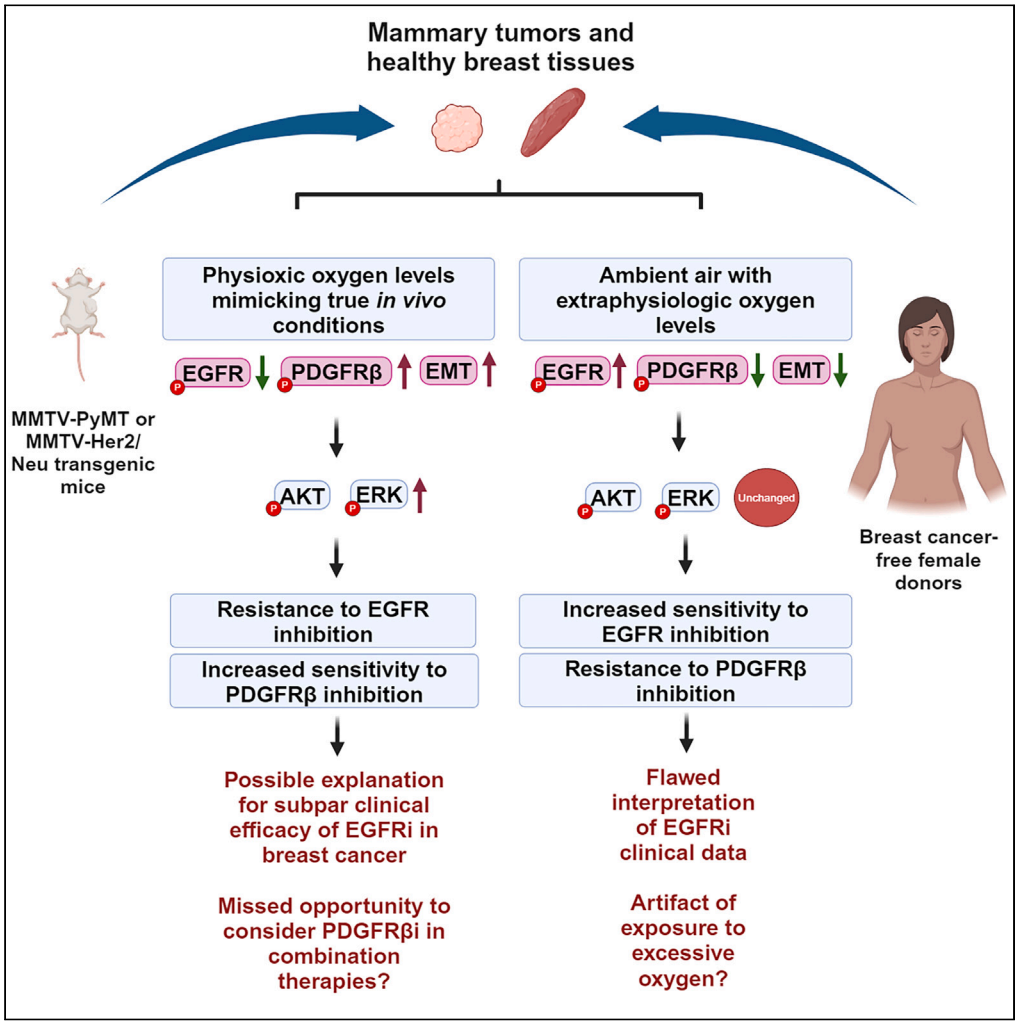

Adedeji K. Adebayo, Poornima Bhat-Nakshatri, Christopher Davis, ..., Brijesh Kumar, Yunlong Liu, Harikrishna Nakshatri

hnakshat@iu.edu

Highlights

Ambient and physioxic oxygen tensions differentially impact cancer cell kinome

PDGFRβ signaling drives response to targeted therapies under physioxia

Combination therapy more effective at physiologic oxygen was identified

Physioxia supports unique epithelial-mesenchymal hybrid cell types

Adebayo et al., iScience 27, 110068
June 21, 2024
https://doi.org/10.1016/j.isci.2024.110068

iScience

CellPress
OPEN ACCESS

Article

Oxygen tension-dependent variability in the cancer cell kinome impacts signaling pathways and response to targeted therapies

Adedeji K. Adebayo,[1,2,3] Poornima Bhat-Nakshatri,[1] Christopher Davis,[4] Steven P. Angus,[3,4] Cihat Erdogan,[5] Hongyu Gao,[5] Nick Green,[5] Brijesh Kumar,[1,7] Yunlong Liu,[5] and Harikrishna Nakshatri[1,2,3,6,8,*]

SUMMARY

Most cells in solid tumors are exposed to oxygen levels between 0.5% and 5%. We developed an approach that allows collection, processing, and evaluation of cancer and non-cancer cells under physioxia, while preventing exposure to ambient air. This aided comparison of baseline and drug-induced changes in signaling pathways under physioxia and ambient oxygen. Using tumor cells from transgenic models of breast cancer and cells from breast tissues of clinically breast cancer-free women, we demonstrate oxygen-dependent differences in cell preference for epidermal growth factor receptor (EGFR) or platelet-derived growth factor receptor beta (PDGFRβ) signaling. Physioxia caused PDGFRβ-mediated activation of AKT and extracellular regulated kinase (ERK) that reduced sensitivity to EGFR and phosphatidylinositol-4,5-bisphosphate 3-kinase catalytic subunit alpha (PIK3CA) inhibition and maintained PDGFRβ+ epithelial-mesenchymal hybrid cells with potential cancer stem cell (CSC) properties. Cells in ambient air displayed differential EGFR activation and were more sensitive to targeted therapies. Our data emphasize the importance of oxygen considerations in preclinical cancer research to identify effective drug targets and develop combination therapy regimens.

INTRODUCTION

Cancer remains one of the biggest threats to global public health today with over 2 million new cancer cases predicted to occur in the United States in the year 2024.[1] A major contributing factor to cancer-related deaths is drug resistance,[2] which has been a major focus of research for many decades. Most notable among these efforts are multiple clinical trials involving various combinations of traditional and targeted therapy regimens.[3,4] In breast cancer, targeted therapies are being developed and/or used toward multiple oncogenic signaling pathways involving receptor tyrosine kinases (RTKs) such as the epidermal growth factor receptor (EGFR) and protein kinases such as protein kinase B (PKB/AKT) and extracellular regulated kinase (ERK).[5] In many cancers, resistance to targeted therapies is mediated via various mechanisms that allow cancer cells to bypass targeted pathways, alter drug targets by activating downstream effectors, or adopt phenotypic changes that contribute to drug resistance.[6] Notably, the crosstalk between the RAF-MEK-ERK and phosphatidylinositol 3-kinase (PI3K)/AKT signaling axis has been demonstrated to contribute to resistance to therapies targeting either pathway.[7–9] Furthermore, recent studies have demonstrated the capacity for targeted therapies to induce resistance by reprogramming the epigenome, transcriptome, and kinome of the cancer cells.[7–9]

Tumor microenvironmental factors are also known to contribute to the behavior of cancer cells and how they respond to targeted therapies. An important characteristic of the tumor microenvironment is its significantly low oxygen (O_2) levels. In solid tumors, O_2 levels are highly variable, with different regions being physioxic (~8% O_2), hypoxic (~1% O_2), or anoxic (~0% O_2), depending on blood (and O_2) supply and rate of O_2 consumption.[10,11] This variability in O_2 distribution is also affected by spatiotemporal fluctuations in O_2 levels in solid tumors in a phenomenon known as cycling hypoxia.[10,12] Despite low tumor O_2 levels, preclinical cancer studies are routinely done in ambient air with O_2 levels (~21%) that significantly exceed the maximum O_2 level tumor cells experience *in vivo*. This is of importance considering the impact that O_2 has on tumor biology[13,14] and important O_2-sensing roles of epigenetic regulators such as KDM5A and KDM6B.[15,16] Although extensive studies have been done to explore the impact of hypoxia on cancer cell behavior in comparison to ambient O_2, termed "normoxia," pioneering studies involving cells of the hematopoietic system revealed that even brief exposure of hematopoietic stem cells to ambient air significantly

[1]Department of Surgery, Indiana University School of Medicine, Indianapolis, IN 46202, USA
[2]Department of Biochemistry and Molecular Biology, Indiana University School of Medicine, Indianapolis, IN 46202, USA
[3]Indiana University Simon Comprehensive Cancer Center, Indiana University School of Medicine, Indianapolis, IN 46202, USA
[4]Department of Pediatrics, Herman B Wells Center for Pediatric Research, Indiana University School of Medicine, Indianapolis, IN 46202, USA
[5]Center for Computational Biology and Bioinformatics, Indiana University School of Medicine, Indianapolis, IN 46202, USA
[6]Roudebush VA Medical Center, Indianapolis, IN 46202, USA
[7]Present address: School of Biomedical Engineering, Indian Institute of Technology (Banaras Hindu University), Varanasi, UP 221005, India
[8]Lead contact
*Correspondence: hnakshat@iu.edu
https://doi.org/10.1016/j.isci.2024.110068

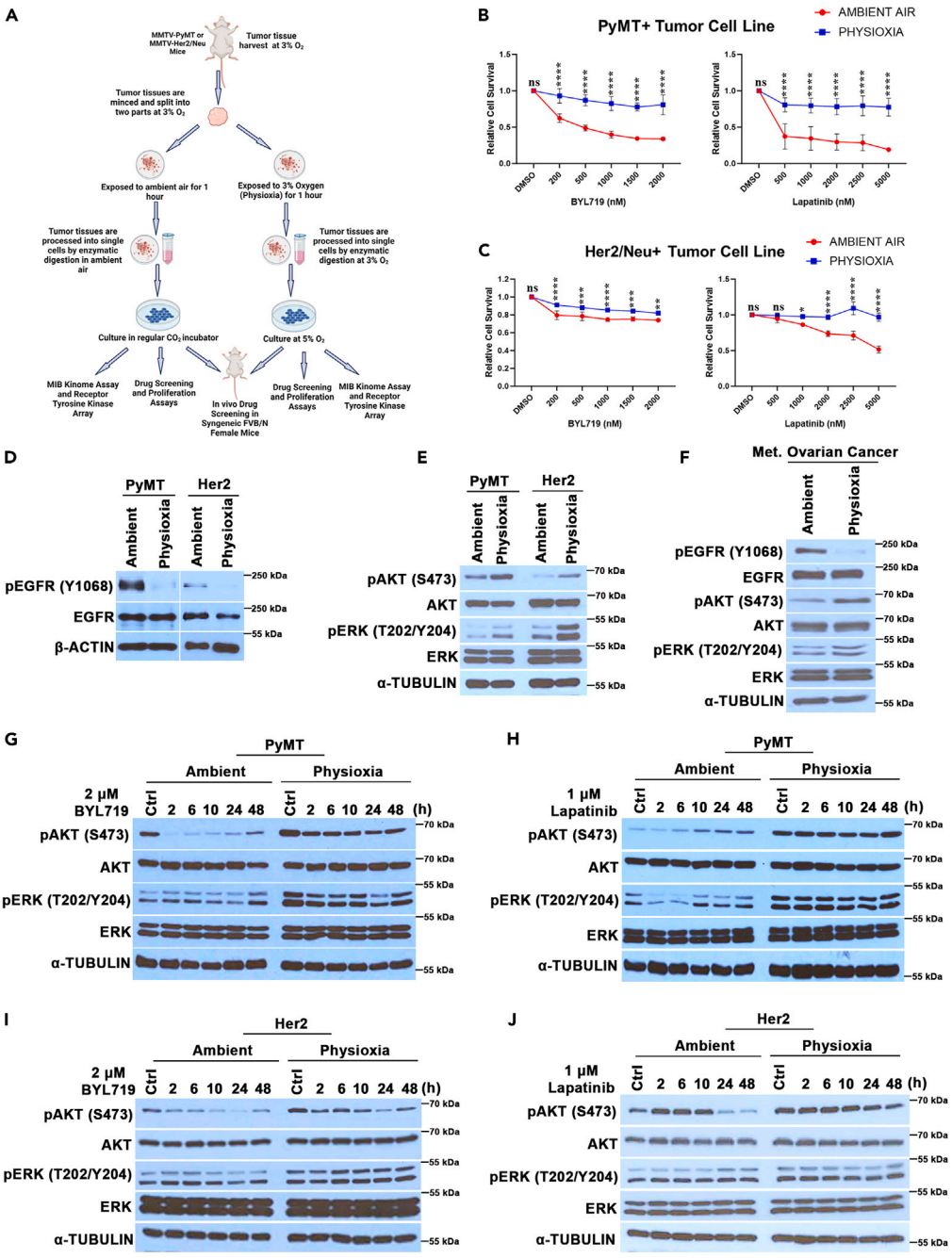

Figure 1. Ambient and physioxic oxygen tensions impact signaling pathways and response to targeted therapies

(A) Schematic representation of experimental workflow (Created with BioRender.com).

(B) Cell proliferation rate of PyMT+ tumor cell lines following treatment with indicated doses of BYL719 (alpelisib) and lapatinib. Proliferation rate was determined using BrdU ELISA (n = 4).

(C) Cell proliferation rate of Her2/Neu+ tumor cell lines following treatment with indicated doses of BYL719 (alpelisib) and lapatinib. Proliferation rate was determined using BrdU ELISA (n = 3).

(D) PyMT+ and Her2/Neu+ tumor cells harvested and processed in physioxia showed lower phosphorylation of EGFR on Y1068.

(E) EGFR's downstream signaling effectors, AKT and ERK showed higher phosphorylation levels under physioxia compared to ambient air.

(F) Phosphorylation status of EGFR and downstream signaling effectors in human metastatic ovarian cancer cell lines in ambient air and physioxia.

(G) Time course assay shows distinct effects of PI3K inhibitor BYL719 on pAKT and pERK levels in PyMT+ cells grown under ambient air and physioxia.

(H) Time course treatment with lapatinib shows minimal impact on phosphorylation of AKT and ERK in PyMT+ tumor cells grown in physioxia compared to ambient air.

Figure 1. *Continued*

(I) Time course assay shows distinct effects of PI3K inhibitor BYL719 on pAKT and pERK levels in Her2/Neu+ cells grown under ambient air and physioxia.
(J) Time course treatment with lapatinib shows minimal impact on phosphorylation of AKT and ERK in Her2/Neu+ tumor cells grown in physioxia. Data in (B) and (C) are presented as means ± SD. Cell proliferation rates were compared with two-way ANOVA, followed by Sidak's multiple comparisons test. *$p < 0.05$, **$p < 0.01$, ***$p < 0.001$, and ****$p < 0.0001$; ns, not significant. Western blot data are representative of at least 3 biologic replicates.

impacts their biology by accelerating their differentiation and limiting their engraftment capabilities.[17,18] This suggests a need for the regulation of experimental O_2 tension in routine *in vitro* and *in vivo* cell manipulations.

Considerations for O_2 among other tumor microenvironmental components become important if one considers the current trends in the failure of clinical trials and issues with data reproducibility. While multiple factors contribute to failure of clinical trials,[19] one fundamental problem is associated with flawed target validation processes that lead to development of drug candidates that lack clinical efficacy.[20] In our previous work, we hypothesized that the characterization of tumor cells under physioxia is crucial to reliably identify changes in tumor biology that impact growth characteristics and sensitivity to targeted therapies. We developed a system that allowed collection, processing, and evaluation of tumor cells under physioxia (3%–5% O_2) such that they had little to no exposure to ambient air.[10,21] We showed O_2-dependent differences in cancer stem cell marker profiles, signaling pathways, tumorigenicity, and response to therapy.[21]

In the present study, our goal was to explore kinome changes and associated signaling pathway alterations that occur in the context of ambient and physioxic O_2 tensions and how these signaling changes impact their response to targeted therapies. By employing a combination of kinome profiling, proteomic, and transcriptomic approaches, we demonstrate distinct differences in the biology of tumor and healthy breast epithelial cells collected, processed, and propagated in ambient air and physioxia. Specifically, we show physioxia-driven changes in the expression and activity of drug targets that are modulated by platelet-derived growth factor receptor beta (PDGFRβ), an RTK. We emphasize that the signaling differences observed under physioxia occur independent of the classical HIF-1α pathway that is typically activated under hypoxic O_2 levels. Our studies reveal a combination therapy regimen that was observed to be efficacious only in tumor cells under physioxia. The effectiveness of this drug combination was made evident by differential pathway activation involving PDGFRβ activity in physioxia that rendered the cells sensitive to treatment. We propose that the collection, processing, culture, and evaluation of cancer cells under physioxia reflects their *in vivo* biology, and adaptation of this additional step is necessary to ensure a more reliable drug development process in preclinical cancer research.

RESULTS

Ambient and physioxic O_2 tensions impact signaling networks and response to targeted drugs

To determine the impact of the differential O_2 tensions on the drug targets and response to targeted drugs, we developed a system with mammary tumors from MMTV-PyMT (mouse mammary tumor virus-polyomavirus middle tumor-antigen) and MMTV-Her2/Neu (human epidermal growth factor receptor 2/Neu) mice (Figure 1A). The MMTV-PyMT transgenic mouse model is a well-characterized mouse model of breast cancer that spontaneously develops mammary tumors. Mammary tumor development in these mice has been reported to be similar to human breast cancer, particularly with regard to patterns of tumor progression and morphological features.[22,23] These tumors are considered to represent the "luminal B" breast cancer subtype.[24] The MMTV-Her2/Neu transgenic mouse model represents *HER2*-amplified breast tumor subtype and is used to study the mechanistic roles of HER2 in breast cancer progression.[25] We harvested tumor tissues from these mice at 3% O_2, macerated the tumor tissues into <1 mm fragments, and split the tissues into two portions. One portion of the tumor tissues was exposed to room O_2 (~21%) for 1 h, while the other portion was left at 3% O_2 for the same duration. We ensured that tissues from the same tumor were used to avoid mouse-to-mouse tumor variabilities that could confound observed effects. Following the 1-h exposure, the tumor tissues were enzymatically dissociated into single cells and cultured at 5% O_2 in a physioxia incubator or 21% O_2 in a regular CO_2 incubator (Figure 1A). The experimental O_2 tensions of 3%–5% and 21% O_2 are referred to as physioxia and ambient air, respectively, from here onward.

We have previously evaluated tumor cells collected, processed, and propagated in ambient air and physioxia and reported significant differences in response to targeted drugs and chemotherapeutic agents.[21] In this study, we re-evaluated the sensitivity of the PyMT+ and Her2/Neu+ mouse tumor cells to the phosphoinositide 3-kinase isoform alpha (PI3Kα) inhibitor BYL719 (alpelisib) and the dual EGFR/HER2 inhibitor lapatinib. Like our previous report, PyMT+ and Her2/Neu+ tumor cells processed and grown in physioxia were less responsive to both drugs compared to those grown in ambient air (Figures 1B and 1C). Based on these data, and the capacity of the differential O_2 tensions to induce significant changes in multiple signaling pathways,[21] we hypothesized that both physioxia and ambient air differentially impact the cancer cell kinome in a manner that influences how sensitive the cells are to targeted therapies. To evaluate the tumor cell kinome in the context of the differential O_2 tensions, we performed an RTK array comparing RTK activity in PyMT mouse tumor cells exposed to ambient air versus physioxia without expansion in culture. We observed lower levels of phosphorylated EGFR and HER2 under physioxia compared to ambient air in PyMT+ tumor cells (Figure S1A). We then confirmed the expression levels of phosphorylated EGFR in both O_2 tensions via western blotting for phospho-EGFR (Y1068). EGFR phosphorylated at Y1068 corresponds to activated EGFR.[26] EGFR phosphorylation on Y1068 was less evident in physioxia compared to ambient air in both the PyMT+ and Her2/Neu+ cells (Figure 1D), suggesting differential activation of EGFR in ambient air relative to physioxia. We also confirmed the differential activation of EGFR in tumor cells expanded in culture in both O_2 tensions to ensure that the observation is consistent in both cultured and uncultured tumor cells (Figure S1B). Evaluation of EGFR mRNA levels showed only a modest decline under physioxia for the PyMT+ tumor cell line, but no significant difference in the Her2/Neu+ cells, suggesting that the observed differences are post-transcriptional (Figure S1C). Surprisingly, the levels of EGFR's downstream effectors, AKT and

ERK, in their activated states were lower in ambient air, compared to physioxia in both cell lines, despite increased EGFR activity (Figure 1E). The phosphorylation of AKT on serine-473 is required for its stabilization and activation.[27,28] Similarly, the phosphorylation of ERK on regulatory sites threonine-202 and tyrosine-204 causes its activation.[29] The differential phosphorylation of AKT and ERK under physioxia, despite decreased EGFR activity, suggests that the activation of these kinases occurred independent of EGFR activation and may be due to the activity of a different component of the kinase signaling cascade that is active in physioxia. Importantly, similar findings were made in human metastatic ovarian cancer cells that were collected, processed, and grown in physioxia and ambient air (Figure 1F). These findings indicate that O_2 tension during tumor tissue collection, processing, and culturing influences the activity of specific kinases in cancer cells.

Tumor cells in ambient air and physioxia show distinct signaling pattern in response to kinase inhibitor treatment

Following the observed resistance of the tumor cells in physioxia to targeted therapies and O_2-dependent differences in phosphorylation status of AKT and ERK, we evaluated the impact of PI3K and EGFR inhibition on activation status of AKT and ERK to determine the influence of O_2 tension on pathway activation upon targeted therapy treatment. In a time-course experiment, we treated PyMT+ tumor cells under physioxia and ambient air with 2 μM BYL719 or 1 μM lapatinib, harvested the cells at the indicated time points, and measured the levels of phospho-AKT (S473) and phospho-ERK (T202/Y204) via western blotting. While BYL719 caused almost complete inhibition of AKT phosphorylation after hours of treatment under ambient air, significant levels of phospho-AKT persisted after 48 h of treatment under physioxia in the PyMT+ cell lines (Figure 1G). Treatment with lapatinib caused a gradual increase in phospho-AKT levels in ambient air, but levels remained unchanged up to 48 h of treatment under physioxia (Figure 1H). Lapatinib reduced phospho-ERK levels only in the cells in ambient air but not under physioxia (Figure 1H). We observed similar effects of BYL719 and lapatinib in Her2+ tumor cells in context of the respective O_2 tensions (Figures 1I and 1J). The PI3K inhibitor effectively inhibited the phosphorylation of AKT in the Her2/Neu+ cells grown in ambient air compared to the cells in physioxia that showed persistent AKT phosphorylation despite treatment (Figure 1I). Similarly, there was a modest decrease in ERK phosphorylation following treatment of the Her2/Neu+ cells in ambient air compared to physioxia (Figure 1I). In contrast to the PyMT+ cells, the Her2/Neu+ cells treated with lapatinib in ambient air showed an initial increase followed by a significant decline in AKT phosphorylation at 24 to 48 h of treatment compared to the cells in physioxia that showed only a modest decline in AKT phosphorylation at the 48-h time point (Figure 1J). However, treatment with lapatinib showed no significant effect in ERK phosphorylation in the Her2/Neu+ cell lines treated in both O_2 tensions (Figure 1J). These findings are consistent with the observed decrease in the sensitivity of the tumor cells under physioxia to lapatinib and BYL719. Our observations suggest that the decreased activity of EGFR in the cells grown in physioxia contributes at least in part to the minimal impact of lapatinib on AKT and ERK phosphorylation and by extension, sensitivity to the drug. Prior reports suggest that EGFR positivity or expression is a weak predictor of response to lapatinib.[30] In addition, the baseline increase in AKT phosphorylation levels in physioxia likely dampens the efficacy of PI3K inhibition. This, therefore, indicates that O_2-mediated changes in kinases such as AKT and ERK are likely to impact the sensitivity of tumor cells to targeted therapies.

Ambient and physioxic O_2 tensions differentially impact tumor cell kinome dynamics

To further investigate the differential impact of ambient air and physioxia on tumor cell signaling, we performed active kinome profiling assays to evaluate baseline and drug-induced adaptive changes in the tumor cell kinome in context of both O_2 tensions. To this end, we performed multiplexed inhibitor beads (MIBs) kinome assay on PyMT+ tumor cells treated either with DMSO or 1 μM lapatinib for 48 h in ambient air and physioxia. The MIBs kinome assay uses type I (ATP-competitive) kinase inhibitors coupled to sepharose beads for the enrichment of kinases based on their activity state, expression level, and affinity for the beads. This approach has been used extensively in the evaluation of drug-induced adaptive kinome changes that contribute to resistance to targeted therapies.[8,31,32] In utilizing this technique, we identified one vehicle control physioxia replicate (Veh. Phy.2) as a clear outlier due to reduced overall MIB binding that caused an obvious disparity from the other two biologic replicates (Figures S2A and S2B). This outlier was removed from further statistical analyses. Data from pairwise comparisons performed prior to outlier removal are shown in Figure S2C. The differential O_2 tensions of ambient air and physioxia induced significant changes in the kinome of the tumor cells (Figure 2A). Pairwise comparison between vehicle control ambient air and physioxia-derived cells revealed increased MIB binding of kinases such as c-KIT, MELK, and TNK1 and a decrease in MIB binding of other kinases including MERTK and PI4K2A in ambient air relative to physioxia (Figure 2B). Notably, removal of the aforementioned outlier revealed a significant decrease in MIB binding of PDGFRβ in the cells under ambient air compared to physioxia (Figures 2A and 2B). c-KIT plays a vital role in proliferation and cell survival, although its role as an oncogene appears to be tissue specific.[33] In breast cancer, loss-of-function mutation of c-KIT and decreases in its expression have been associated with oncogenic transformation of breast epithelial cells and tumor development.[34,35] We confirmed the differential phosphorylation of c-KIT in ambient air (Figure S2D), but its role in the context of the differential O_2 tensions is yet to be determined.

Interestingly, despite increased sensitivity of tumor cells in ambient air to lapatinib, we observed minimal lapatinib-induced changes in the kinome of the tumor cells in the context of ambient air or physioxia (Figure 2C) with the most significant kinome changes occurring due to O_2 level differences rather than lapatinib as seen in Figure 2A. Furthermore, comparison between lapatinib-treated physioxia and ambient air cells showed kinome changes similar to those observed with comparisons between the vehicle controls with increased MIB binding of PDGFRβ in cells treated with lapatinib under physioxia (Figure 2D). PDGFRβ is an RTK that is known to be expressed in tumor stromal cells of mesenchymal origin.[36] Its expression in breast cancer cells has been associated with late-stage tumors with increased metastatic potential.[37,38] Importantly, PDGFRβ in its activated state triggers the activity of downstream signaling effectors, including AKT and ERK, which contributes to tumor cell survival, metastasis, and resistance to some targeted therapies.[39,40] For this reason, we hypothesized that the activation

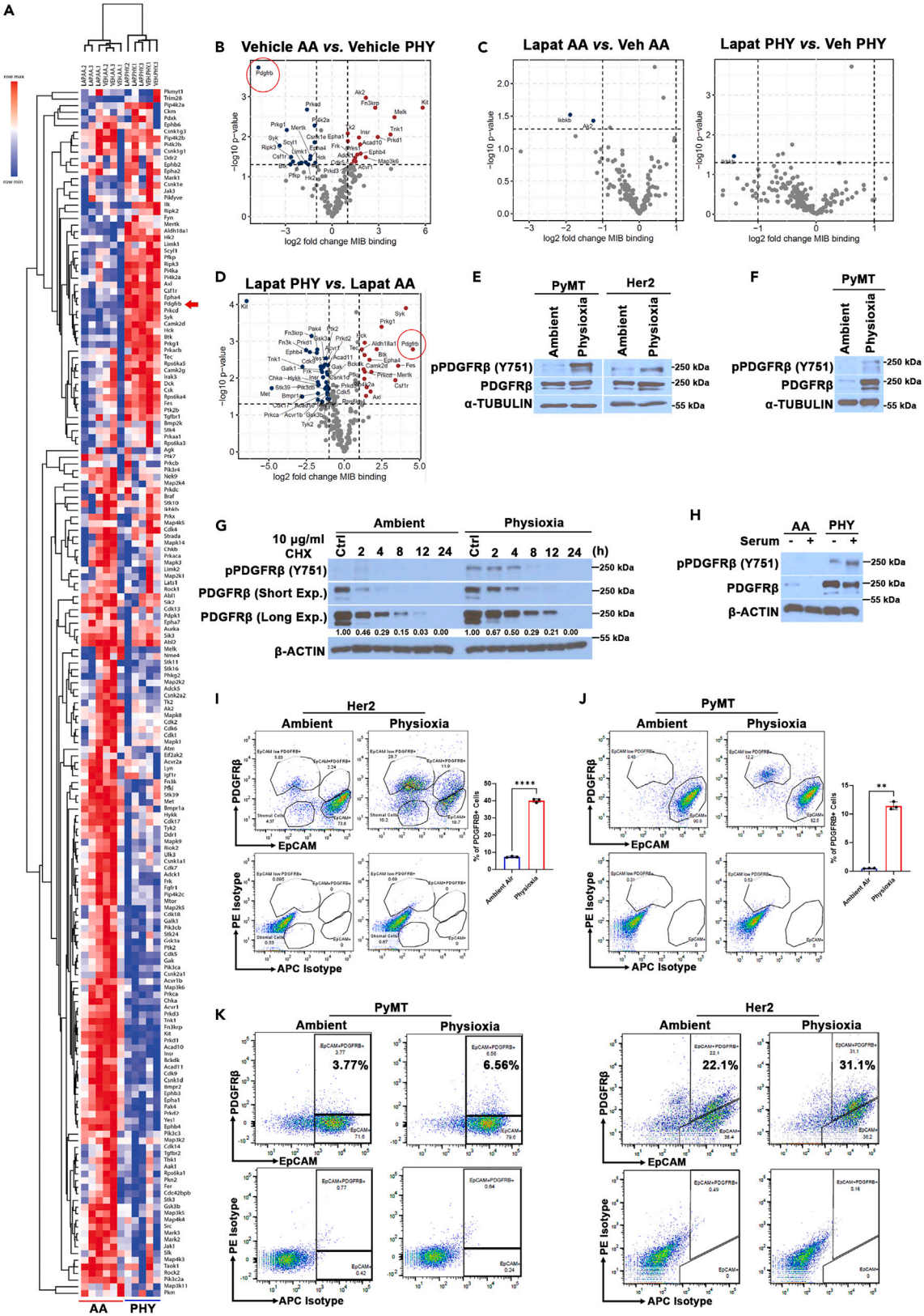
A
AA
PHY
B Vehicle AA vs. Vehicle PHY
log2 fold change MIB binding
−log10 p-value
C Lapat AA vs. Veh AA
Lapat PHY vs. Veh PHY
D Lapat PHY vs. Lapat AA
E
PyMT
Her2
Ambient
Physioxia
pPDGFRβ (Y751)
PDGFRβ
α-TUBULIN
250 kDa
55 kDa
F
G
10 μg/ml CHX
Ctrl 2 4 8 12 24 (h)
PDGFRβ (Short Exp.)
PDGFRβ (Long Exp.)
β-ACTIN
H
Serum
AA PHY
I
J
EpCAM
PDGFRβ
PE Isotype
APC Isotype
% of PDGFRB+ Cells
K
3.77%
6.56%
22.1%
31.1%

Figure 2. Effects of ambient air and physioxia on tumor cell kinome dynamics

(A) Heatmap showing kinome dynamics in PyMT+ mouse tumor cells in ambient air and physioxia based on MIB kinome screening. Red arrow indicates PDGFRβ in the heatmap.

(B) Pairwise comparison between vehicle-treated cells in ambient air and physioxia shows significant differences in bound kinases in PyMT+ tumor cell lines. PDGFRβ is highlighted in red circle.

(C) Treatment of PyMT+ tumor cell lines with 1 μM lapatinib shows minimal kinome changes in ambient air and physioxia.

(D) Pairwise comparison between lapatinib-treated PyMT+ cells in physioxia and ambient air showed differential binding of PDGFRβ under physioxia. PDGFRβ is highlighted in red circle.

(E) Western blot confirms differential phosphorylation of PDGFRβ on Y751 in PyMT+ and Her2/Neu+ cell lines under physioxia compared to ambient air.

(F) Late passage PyMT+ tumor cell lines show lower levels of total PDGFRβ protein in ambient air, compared to physioxia.

(G) Treatment of PyMT+ cells in respective oxygen tensions with cycloheximide at 10 μg/mL shows slower PDGFRβ turnover rate under physioxia compared to ambient air.

(H) Effect of serum starvation on phosphorylation of PDGFRβ on Y751 and total PDGFRβ protein levels in PyMT+ tumor cell lines.

(I) Her2/Neu+ tumor cell lines in physioxia show a higher enrichment of PDGFRβ$^+$ cells compared to ambient air. Graph (right) shows proportion of PDGFRβ$^+$ in ambient air and physioxia (n = 3).

(J) PyMT$^+$ tumor cell lines in physioxia show a higher enrichment of PDGFRβ$^+$ cells compared to ambient air. Graph (right) shows proportion of PDGFRβ$^+$ in ambient air and physioxia (n = 3).

(K) Data show enrichment of EpCAM$^+$/PDGFRβ$^+$ cells in PyMT+ and Her2/Neu+ mouse tumors. Unlike in I and J, cells freshly isolated from tumors without culturing were analyzed. Data are presented as means ± SD. Statistical significance was determined with a two-tailed Student's t test. $^{**}p < 0.01$ and $^{****}p < 0.0001$. Western blot data are representative of at least 3 biologic replicates.

of PDGFRβ in physioxia may contribute to the differential activity of AKT and ERK relative to ambient air. Therefore, we employed two approaches to confirm activation of PDGFRβ under physioxia. First, we carried out an RTK screening using an RTK array kit, with lysates prepared from PyMT+ cells cultured in ambient air and physioxia and treated either with 1 μM lapatinib or vehicle control. We observed increased levels of phosphorylated PDGFRβ in both vehicle control and lapatinib-treated cells cultured in physioxia compared to ambient air (Figure S2E). To confirm that this phosphorylation of PDGFRβ causes its activation, we measured levels of PDGFRβ phosphorylated on tyrosine-751 in the cells grown in both O_2 tensions via western blotting. Phospho-PDGFRβ (Y751) represents an active autophosphorylated PDGFRβ to which PI3K docks and activates AKT signaling.[41,42] Indeed, phospho-PDGFRβ (Y751) was increased in physioxia, compared to ambient air, both in the PyMT+ and the Her2/Neu+ cell lines (Figure 2E). To determine if PDGFRβ phosphorylation in physioxia is due to autocrine release of platelet-derived growth factor (PDGF)-BB cytokine, serum-free culture supernatants of the PyMT+ cells cultured in physioxia and ambient air were screened for cytokines/growth factors, using a cytokine array kit. However, we found no expression of PDGF-BB in the supernatants of the cells cultured under both O_2 tensions (Figure S2F). The same observation was made for epidermal growth factor (EGF) (Figure S2F). This implies that the differential activation of EGFR and PDGFRβ in ambient air and physioxia, respectively, is constitutive and is unlikely due to autocrine or paracrine release of the corresponding growth factors. Interestingly, PDGFRβ in the PyMT+ tumor cell lines was unstable in ambient air as its expression decreased with prolonged culture and multiple passages at 21% O_2 (Figure 2F). This decline in PDGFRβ protein expression appeared to begin at passage numbers ranging from the fourth to fifth and varied with tumors from different mice. To evaluate the stability of PDGFRβ in both O_2 tensions, we treated PyMT+ cells grown in ambient air and physioxia with cycloheximide (CHX), an inhibitor of protein synthesis, over a period of 24 h. CHX was used at 10 and 50 μg/mL and cells were harvested at 2, 4, 8, 12, and 24 h of treatment (final time point was at 12 h for the cells treated with 50 μg/mL CHX). At 2 h of treatment with 10 μg/mL CHX, PDGFRβ protein levels were reduced to less than 50%, relative to control in ambient air, whereas, in physioxia, levels remained up to 67% at the same time point (Figure 2G). PDGFRβ protein levels persisted for at least 12 h in the cells under physioxia, while cells in ambient air exhibited almost complete decline in PDGFRβ protein after 8 h of treatment with CHX (Figure 2G). Similar observations were made in cells treated with 50 μg/mL CHX in both O_2 tensions (Figure S2G). These results suggest longer PDGFRβ half-life under physioxia compared to ambient air. Furthermore, we observed that culture in serum-containing media enhanced PDGFRβ phosphorylation in physioxia, with a concurrent decline in total PDGFRβ levels (Figure 2H). This implies that while there is a baseline activation of PDGFRβ in physioxia, certain growth factor(s) in serum-containing media enhance this activity, with eventual proteasomal degradation of the activated receptor.

Next, we applied flow cytometry to evaluate the cell surface expression of PDGFRβ using freshly processed early (second) passage tumor cells grown in ambient air and physioxia. The Her2/Neu+ cell lines that were grown in physioxia were found to segregate into four distinct populations, namely: EpCAM$^+$, EpCAM$^+$/PDGFRβ$^+$, EpCAM^{low}/PDGFRβ$^+$, and an EpCAM$^-$ stromal cell population (Figure 2I). Importantly, the Her2/Neu+ cells in ambient air had most of the cells enriched in the EpCAM$^+$ populations with significantly fewer cells in the EpCAM$^+$/PDGFRβ$^+$ and EpCAM^{low}/PDGFRβ$^+$ cell populations compared to physioxia (Figure 2I). Similarly, the PyMT+ cells in ambient air were predominantly EpCAM$^+$, with significantly fewer EpCAM^{low}/PDGFRβ$^+$ cells compared to the cells under physioxia (Figure 2J). Regardless of cell line, the proportion of PDGFRβ$^+$ tumor cells was higher in physioxia than in ambient air (Figures 2I and 2J). This suggests that the collection, processing, and propagation of tumor cells in physioxia not only causes PDGFRβ activation, but also contributes to the enrichment of PDGFRβ$^+$ cells. The observed decrease in the enrichment of PDGFRβ$^+$ cells in ambient air, despite relatively equal total PDGFRβ protein expression, is probably due to the faster PDGFRβ turnover rate observed in ambient air. We speculate that ambient O_2 tension contributes to faster internalization and lysosomal degradation of PDGFRβ due to mechanisms that are yet to be determined.

To determine if PDGFRβ$^+$ cells are intrinsically present in the tumors, we processed PyMT+ and Her2/Neu+ mammary tumors as previously described and stained the cells with PDGFRβ and EpCAM fluorescent-conjugated antibodies without culturing the cells. EpCAM$^+$/PDGFRβ$^+$

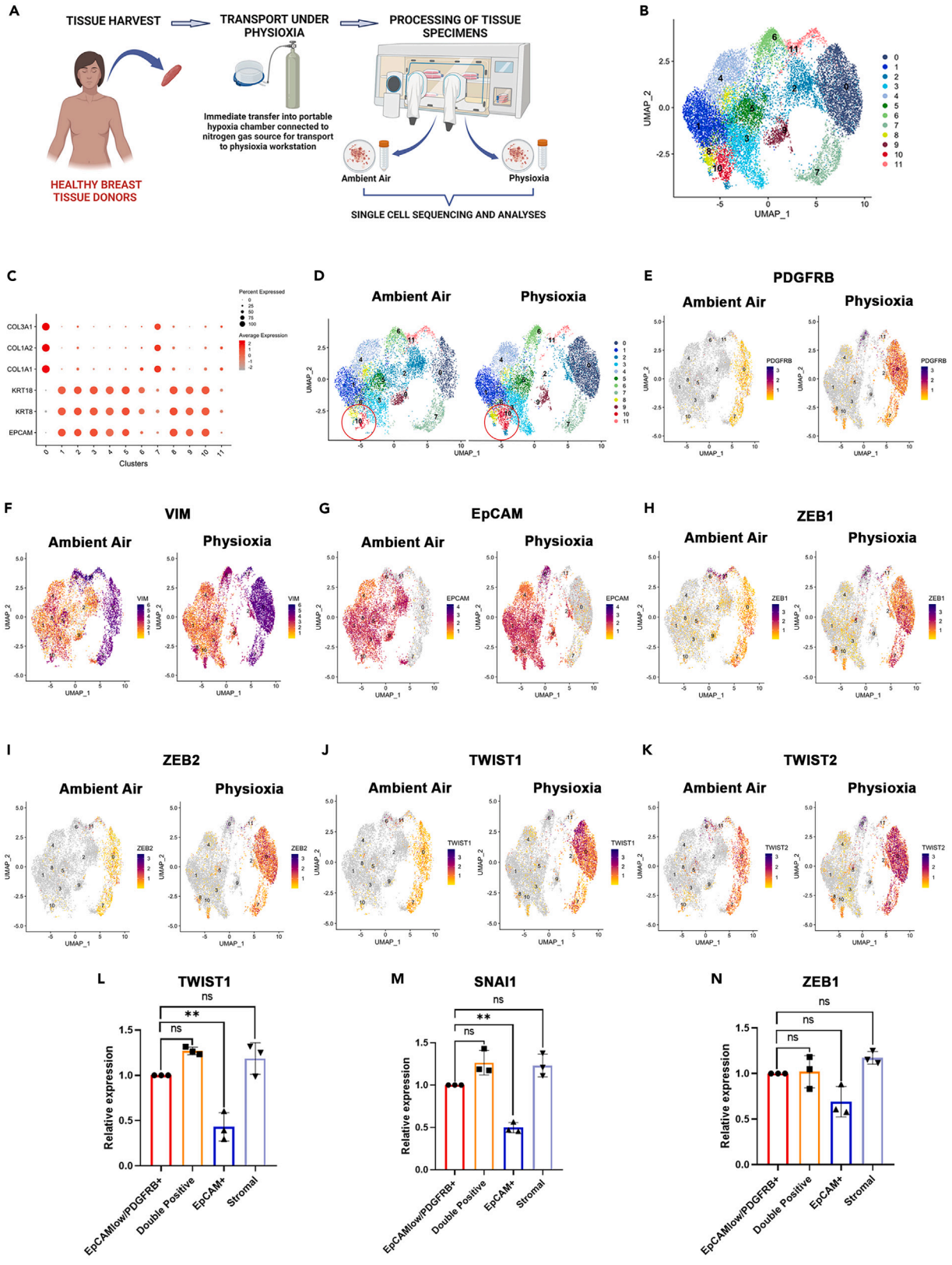
A
TISSUE HARVEST
TRANSPORT UNDER PHYSIOXIA
PROCESSING OF TISSUE SPECIMENS
Immediate transfer into portable hypoxia chamber connected to nitrogen gas source for transport to physioxia workstation
HEALTHY BREAST TISSUE DONORS
Ambient Air
Physioxia
SINGLE CELL SEQUENCING AND ANALYSES
B
UMAP_1
UMAP_2
C
COL3A1
COL1A2
COL1A1
KRT18
KRT8
EPCAM
Clusters
Percent Expressed
Average Expression
D
Ambient Air
Physioxia
E
PDGFRB
Ambient Air
Physioxia
F
VIM
Ambient Air
Physioxia
G
EpCAM
Ambient Air
Physioxia
H
ZEB1
Ambient Air
Physioxia
I
ZEB2
Ambient Air
Physioxia
J
TWIST1
Ambient Air
Physioxia
K
TWIST2
Ambient Air
Physioxia
L
TWIST1
M
SNAI1
N
ZEB1
Relative expression
ns
**
EpCAMlow/PDGFRB+
Double Positive
EpCAM+
Stromal

Figure 3. Single cell RNA-sequencing shows the impact of ambient air and physioxia on expression of *PDGFRβ* and other genes associated with epithelial to mesenchymal transition in primary human breast epithelial cells

(A) Schematic representation of experimental workflow (Created with BioRender.com).

(B) Normal breast epithelial cells cluster into 11 distinct clusters with single-cell RNA sequencing analysis.

(C) Dot blot shows distribution of cell types across all clusters based on expression of indicated marker genes (D) Separation of samples by condition shows differences in clustering patterns based on oxygen tension. Note cell populations unique to physioxia (circled).

(E) UMAP plot shows *PDGFRβ* expression pattern across clusters. Portions of epithelial cells unique to physioxia express *PDGFRβ* also.

(F) UMAP plot shows *VIM* expression pattern across clusters. *VIM* expression is high in *PDGFRβ* expressing epithelial and mesenchymal cell types.

(G) UMAP plot shows *EpCAM* expression pattern across clusters. Unique *PDGFRβ*-expressing cells in physioxia also express *EpCAM*.

(H) Cells expressing *PDGFRβ* show increased expression of EMT marker gene *ZEB1* regardless of epithelial marker gene expression.

(I) Cells expressing *PDGFRβ* show increased expression of EMT marker gene *ZEB2* regardless of epithelial marker gene expression.

(J) Cells expressing *PDGFRβ* show increased expression of EMT marker gene *TWIST1* regardless of epithelial marker gene expression.

(K) Cells expressing *PDGFRβ* show increased expression of EMT marker gene *TWIST2* regardless of epithelial marker gene expression.

(L) qRT-PCR shows relative expression levels of *Twist1* in subtypes of Her2/Neu+ tumor cell lines based on EpCAM and PDGFRβ expression profile ($n = 3$).

(M) qRT-PCR shows relative expression levels of *Snai1* in subtypes of Her2/Neu+ tumor cell lines based on EpCAM and PDGFRβ expression profile ($n = 3$).

(N) qRT-PCR shows relative expression levels of *Zeb1* in subtypes of Her2/Neu+ tumor cell lines based on EpCAM and PDGFRβ expression profile ($n = 3$). Data are presented as means ± SD. Gene expression levels across all groups were compared with one-way ANOVA, followed by Tukey's multiple comparisons test. $^{**}p < 0.01$; ns, not significant.

cells were present at both O_2 tensions in the PyMT+ and Her2/Neu+ tumors, albeit to a lesser extent in the PyMT+ tumors (Figure 2K). Furthermore, EpCAM$^+$/PDGFRβ$^+$ cells were modestly higher in physioxia, compared to ambient air in both mouse models (Figure 2K). These results suggest that culture under physioxic O_2 tension supports the maintenance and enrichment of PDGFRβ$^+$ cells, while ambient air causes their depletion.

Altogether, these findings demonstrate a significant impact of ambient and physioxic O_2 tensions on the tumor cell kinome and reveal a previously unreported effect of O_2 tension on the cell surface levels of PDGFRβ and its activity.

Ambient and physioxic O_2 tensions induce transcriptional changes relevant to epithelial-to-mesenchymal transition in human breast cells

To extend the aforementioned findings to cells of human origin, we devised a means to collect breast biopsies from clinically breast cancer-free women under physioxia. The tissues were collected from two donors via core needle biopsy and transferred immediately (<30 s) into a portable physioxia chamber set to 3% O_2. This chamber was used to transport the collected tissue to the physioxia workstation within minutes (<10 min) of collection. The tissues were processed as described for the tumor tissues and expanded in culture in ambient O_2 and physioxia (additional details in STAR Methods section) (Figure 3A). Following expansion of the breast epithelial cells, we subjected the cultured cells to single-cell RNA sequencing (scRNA-seq) to explore transcriptional changes in the context of the differential O_2 tensions. Integrative analyses of scRNA-seq data from ambient air and physioxia-derived cells revealed 11 major clusters, via a uniform manifold approximation and projection (UMAP) output (Figures 3B and S3A). The list of differentially expressed genes in each cluster can be found in Tables S1 and S2. We identified the cell types that make up each of these clusters by evaluating epithelial and fibroblast/mesenchymal marker genes. We selected *EPCAM*, *KRT8*, and *KRT18* as epithelial marker genes and *COL1A1*, *COL1A2*, and *COL3A1* as fibroblast/mesenchymal marker genes. Based on the expression patterns of these markers, we identified cells in clusters 0, 7, and 11 as mesenchymal, and cells in clusters 1, 2, 3, 4, 5, 6, 8, 9, and 10 as epithelial cells (Figures 3C, S3B, and S3C). Sample separation by O_2 tension revealed few differences in clustering patterns in ambient air and physioxia. Notably, we observed a higher number of cells in cluster 2 in ambient air compared to physioxia (Figure 3D). However, this observation was not consistent in the two ambient air-derived samples suggesting individual donor differences in cell population (Figure S3A). Interestingly, portions of the epithelial cells in clusters 8 and 10 that are present in the physioxia-derived cells were absent in ambient air (Figure 3D). This population was also observed to be composed of portions of cluster 2, suggesting transcriptional similarities among these cells (Figure 3D). We then focused on *PDGFRβ*. As expected, the mesenchymal cells in clusters 0, 7, and 11 expressed high levels of *PDGFRβ*, compared to the epithelial cell clusters (Figure 3E). Furthermore, levels of *PDGFRβ* in these mesenchymal cell types appeared to be much higher in the physioxia-derived cells, compared to ambient air, consistent with the previously observed stable PDGFRβ expression in the tumor cells under physioxia (Figure 3E). The aforementioned portions of epithelial cell clusters 2, 8, and 10 also exhibited high *PDGFRβ* levels comparable to the mesenchymal cell clusters (Figure 3E). This is consistent with the expression of *VIM* and other mesenchymal marker genes *COL1A1*, *COL1A2*, and *COL3A1* (Figures 3F and S3B) in these cells. These cells are unique in that, in addition to the fibroblast/mesenchymal markers, they also express epithelial marker genes such as *EPCAM*, *KRT8*, and *KRT18* and are only enriched in physioxia (Figures 3G and S3B). This finding is in line with the enrichment of PDGFRβ$^+$/EpCAM$^+$ Her2/Neu+ mammary tumor cells under physioxia, further supporting the notion that physioxic culture conditions support the growth of these unique epithelial-mesenchymal hybrid cell types which are known to be metastasis-competent cancer stem cells.[43] A recent study of major epithelial cell types of mouse mammary gland showed the expression of PDGFRβ protein in basal-myoepithelial cells, almost to levels observed in fibroblasts.[44] Similar to basal-myoepithelial cells, a fraction of cells in cluster 6 expressed both *PDGFRβ* and *KRT14* under physioxia (Figure S3D). Furthermore, cluster 9 cells under physioxia expressed higher levels of *KRT14* compared to those in ambient air (Figure S3D).

Based on the mesenchymal phenotype of the *PDGFRβ*-expressing cells, we reasoned that these cells are likely to express genes known to regulate epithelial-to-mesenchymal transition (EMT). Indeed, the *PDGFRβ*-expressing cells, regardless of epithelial marker gene expression,

were found to express significant levels of EMT marker genes including *ZEB1*, *ZEB2*, *TWIST1*, *TWIST2*, and *SNAI2* (*SLUG*) (Figures 3H–3K and S3E). To determine whether the EMT-related transcriptional changes that were observed in the healthy human breast epithelial cell lines were also relevant in tumor cells, we flow sorted Her2/Neu+ mouse tumor cells grown in physioxia using PDGFRβ and EpCAM fluorescent-conjugated antibodies. The sorted cells were then expanded in culture under physioxia for quantitative reverse-transcription PCR analyses of EMT-transcription factors (TFs). The sorted cell populations exhibited distinct morphologies, with the EpCAM^{low}/PDGFRβ^{+} cell populations displaying mesenchymal morphology, and the EpCAM^{+} and EpCAM^{+}/PDGFRβ^{+} populations displaying epithelial morphology (Figure S4). We evaluated the different populations of the Her2/Neu+ cells for expression levels of *Twist1*, *Zeb1*, and *Snai1*, with the expression levels measured relative to the EpCAM^{low}/PDGFRβ^{+} cell populations. We observed that the EpCAM^{+}/PDGFRβ^{+} and EpCAM^{low}/PDGFRβ^{+} Her2/Neu+ cell populations expressed significantly higher levels of *Twist1* and *Snail1* compared to the EpCAM^{+} cell populations (Figures 3L and 3M). A similar trend was observed for *Zeb1*, though not statistically significant (Figure 3N). These findings suggest a potential role for PDGFRβ signaling in the adoption of the epithelial-mesenchymal hybrid state in populations of Her2/Neu+ mammary tumor cells that are collected, processed, and grown in physioxia. Notably, recent studies have demonstrated the potential role of TWIST1 in transcriptional activation of the PDGFRβ promoter in breast cancer cells and cancer stem cell populations to enhance tumorigenicity, tumor cell migration, and metastasis.[45] Consistent with findings from the scRNA-seq analysis of the breast epithelial cells (Figures 3H–3K), the EpCAM^{-} stromal/fibroblast cell population expressed similar levels of the EMT-TFs as the EpCAM^{+}/PDGFRβ^{+} and EpCAM^{low}/PDGFRβ^{+} cell populations (Figures 3L–3N). Thus, expression levels of the EMT-TFs measured through bulk RNA-seq of tumors may not truly represent levels in tumor cells and in large part may come from stromal cell populations, including cancer-associated fibroblasts, within the tumor microenvironment.[46]

O_2 tension-dependent signaling by PDGFRβ influences sensitivity of tumor cells to targeted therapies

Based on the observed differential phosphorylation of PDGFRβ in physioxia, and the reported impact of PDGFRβ signaling on downstream signaling pathways,[38,39] we determined whether the activation of PDGFRβ contributed to differential AKT and ERK signaling under physioxia. To this end, we treated PyMT+ mouse tumor cells with three kinase inhibitors imatinib (5 μM), sorafenib (2 μM), and sunitinib (2 μM) to determine which of these drugs could more effectively inhibit PDGFRβ and if PDGFRβ inhibition showed any effect on downstream AKT and ERK signaling. The rationale for testing three different kinase inhibitors is based on the lack of a kinase inhibitor that is specific for PDGFRβ.[47] Of these three drugs, only sunitinib effectively inhibited the phosphorylation of PDGFRβ on Y751 in the PyMT+ cells under physioxia (Figure 4A). In addition to the dephosphorylation of PDGFRβ by sunitinib, there was a concurrent inhibition of AKT, although ERK phosphorylation was not impacted (Figure 4A). Since sunitinib has additional targets, including c-KIT and the vascular endothelial growth factor receptors (VEGFRs),[48] we reasoned that the effect of PDGFRβ inhibition may also be due to off-target effects. Therefore, to inhibit PDGFRβ specifically, we performed transient knockdown of *Pdgfrb* in the PyMT+ and the Her2/Neu+ tumor cells. As observed with pharmacologic inhibition of PDGFRβ, transient depletion of PDGFRβ levels by RNA interference led to a concurrent decrease in the phosphorylation of AKT in the PyMT+ and the Her2/Neu+ tumor cell lines (Figure 4B). Interestingly, genetic inhibition of PDGFRβ in the PyMT+ cells also decreased ERK phosphorylation. However, this impact on ERK phosphorylation was not observed in the Her2/Neu+ cell lines following *Pdgfrb* knockdown (Figure 4B). We speculate that in the context of physioxic O_2 tension, while PDGFRβ may have a direct impact on the activity of AKT, the effect on ERK signaling may be partial and is probably oncogene dependent. Alternatively, the interaction between PDGFRβ and ERK signaling is likely to be complex and mediated by other effectors under the influence of PDGFRβ activity.[49] Since both pharmacologic and genetic inhibition of PDGFRβ caused a decline in AKT phosphorylation and partially impacted ERK signaling under physioxia, we hypothesized that the tumor cells grown in physioxia are more sensitive to treatment with sunitinib. To assess this possibility, we treated PyMT+ tumor cells with the indicated doses of sunitinib for 48 h and evaluated cell survival via bromodeoxyuridine (BrdU) enzyme-linked immunosorbent assay (ELISA). We found that the tumor cells grown under physioxia are more sensitive to sunitinib treatment compared to the cells in ambient air, which showed minimal response to the drug (Figure 4C).

Because the tumor cells grown in physioxia were sensitive to sunitinib treatment, we reasoned that the combination of sunitinib and lapatinib would render the tumor cells grown in physioxia more sensitive to treatment compared to single treatment with either drug. Therefore, we treated PyMT+ tumor cells grown in ambient and physioxic O_2 tensions with 1 μM lapatinib and sunitinib, both singly and in combination. We observed that a combination of lapatinib and sunitinib had a significant effect on tumor cell survival in physioxia than either drug alone (Figure 4D). However, in the ambient air tumor cells, there was no significant difference in sensitivity to treatment with lapatinib alone and a combination of lapatinib and sunitinib (Figure 4D). We then utilized the SynergyFinder+ web application[50] to determine the type of drug interaction between the two drugs in the context of the respective O_2 tensions, following treatment with various drug doses either alone or in combination. Bliss independence analysis with this tool revealed more synergistic growth inhibition with lapatinib and sunitinib combination in physioxia than in ambient air, with Bliss synergy scores of 5.52 and 54.43 in ambient air and physioxia, respectively (Figures 4E and S5A). To determine if apoptosis plays any role in the observed cell death following treatment, we treated PyMT+ cells with lapatinib and sunitinib, both singly and in combination for a period of 48 h and analyzed cell lysates for caspase-3 activity. As expected, single treatment with lapatinib led to higher caspase-3 activity relative to vehicle control in ambient air compared to physioxia (Figure 4F), suggesting that the ability of lapatinib to induce apoptosis is blocked by signaling pathways active under physioxic growth conditions. Importantly, the combination of lapatinib and sunitinib enhanced caspase-3 activity in both O_2 tensions (Figure 4F). To evaluate the expression of additional mediators of apoptosis upon treatment and in context of ambient and physioxic O_2 tensions, we subjected lysates derived from PyMT+ cells treated with lapatinib and sunitinib, singly and in combination in both ambient air and physioxia to an apoptosis array. The apoptosis array showed a decline in the expression of the antiapoptotic proteins Mcl-1, Bcl-2, Bcl-x, and claspin following treatment of PyMT+ cells with a combination

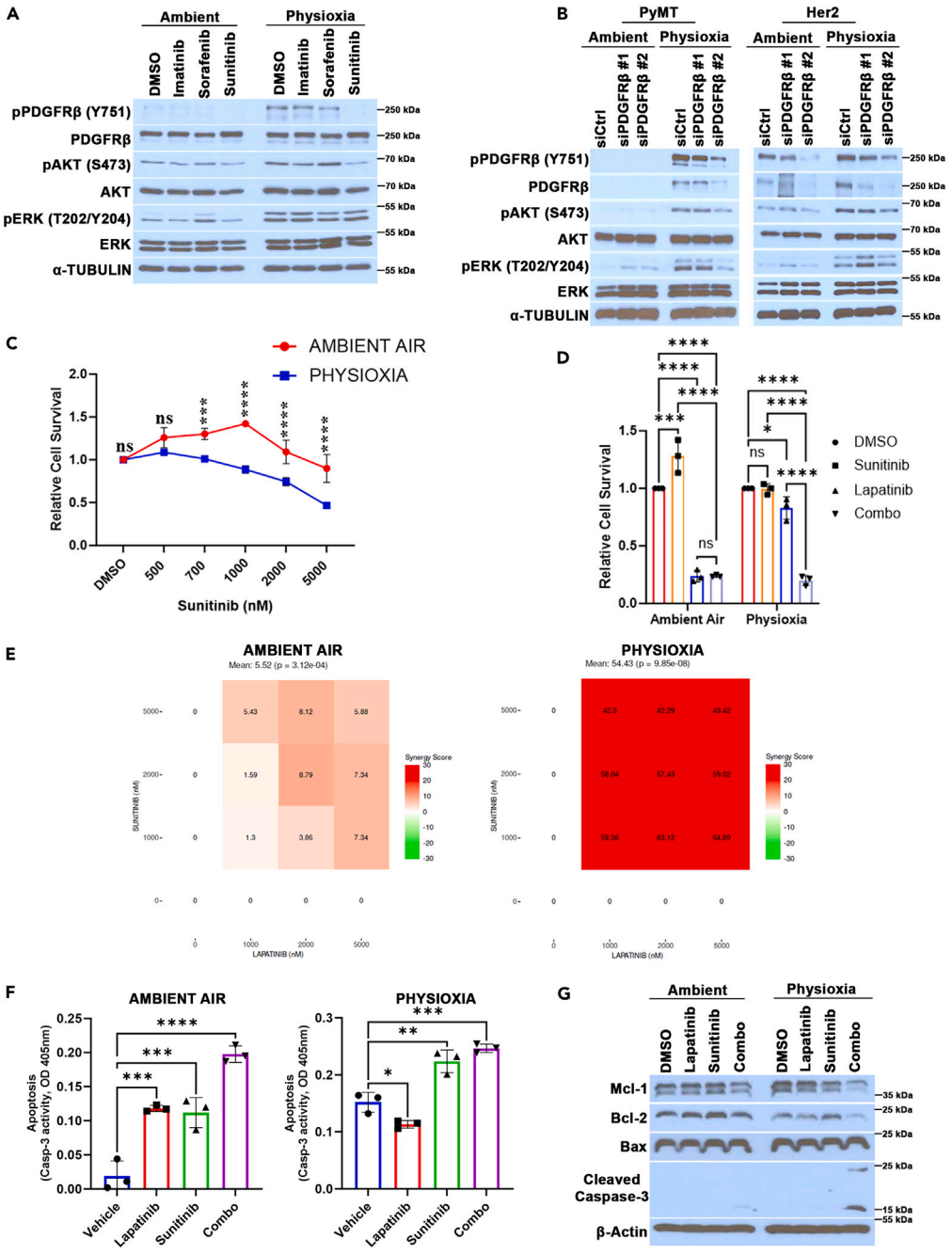

Figure 4. Oxygen-dependent signaling by PDGFRβ influences sensitivity of tumor cells to targeted drugs and combination therapy

(A) Treatment of PyMT+ tumor cells with 2 μM sunitinib concurrently inhibits phosphorylation of PDGFRβ and AKT on Y751 and S473, respectively, in physioxia.

(B) Transient knockdown of PDGFRβ causes inhibition of AKT and ERK phosphorylation in PyMT+ cell lines (left) and only AKT in Her2/Neu+ cell lines (right).

(C) Cell proliferation rate of PyMT+ tumor cell lines following treatment with indicated doses of sunitinib. Proliferation rate was determined using BrdU ELISA ($n = 3$).

(D) The effects of sunitinib, lapatinib, and combination treatment on proliferation of PyMT+ cells maintained under ambient air and physioxia ($n = 3$).

(E) Bliss independence analysis reveals synergistic growth inhibition with lapatinib and sunitinib combination with higher synergy score under physioxia compared to ambient air.

(F) The effects of sunitinib, lapatinib, and combination treatment on caspase-3 activity in PyMT+ cell lines ($n = 3$).

(G) Combination of lapatinib and sunitinib decreases expression of the antiapoptotic proteins Mcl-1 and Bcl-2, with associated increase in caspase-3 activity under physioxia. Comparison of cell proliferation rates in (C) and (D) was done with two-way ANOVA and Sidak's multiple comparisons post hoc test. Caspase-3 activity in (F) was compared with one-way ANOVA, followed by Tukey's multiple comparisons test. Data are presented as means ± SD. *$p < 0.05$, **$p < 0.01$, ***$p < 0.001$, and ****$p < 0.0001$; ns, not significant.

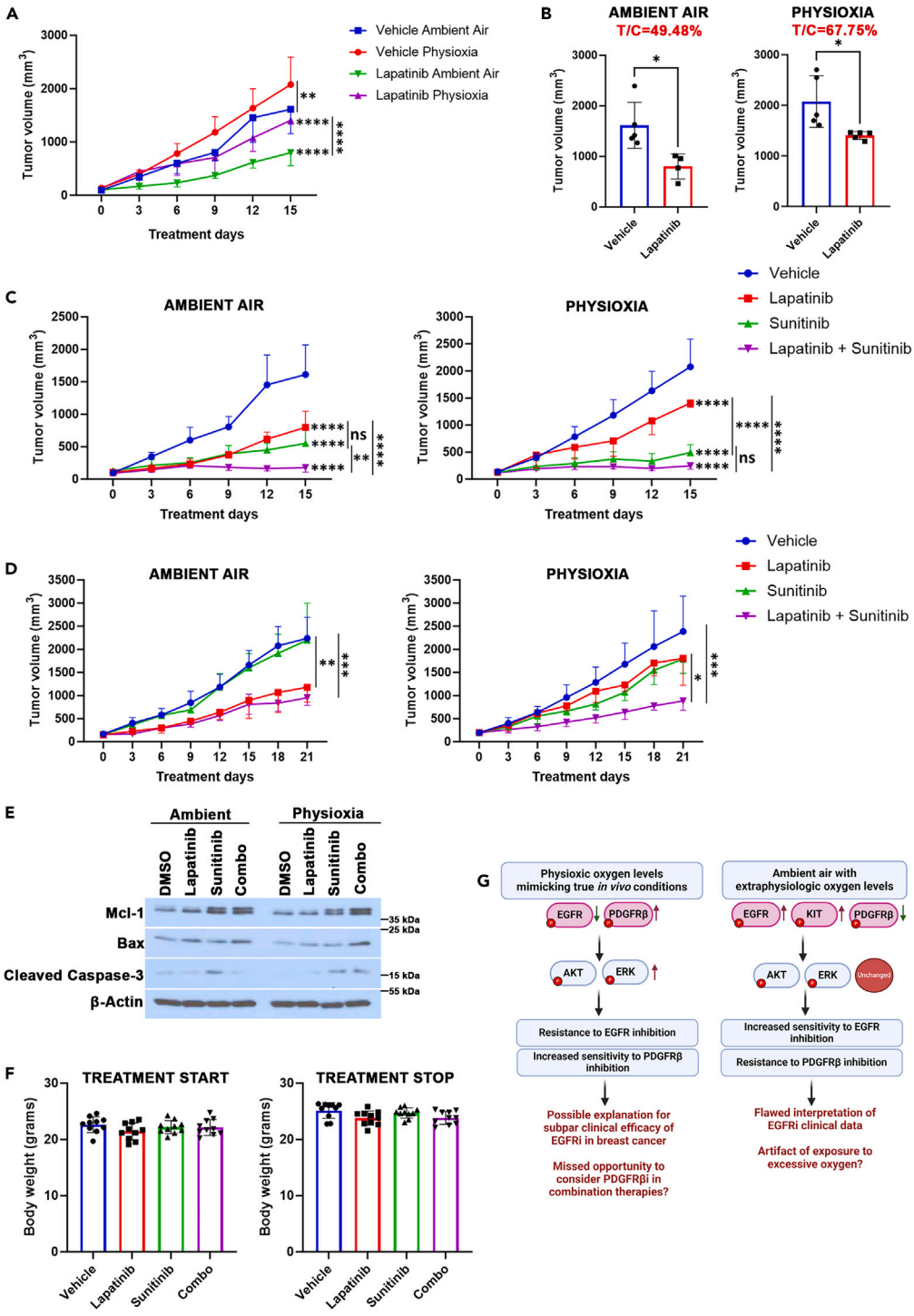

Figure 5. Tumors established from tumor cells grown under physioxia and ambient air show differential sensitivity to concurrent PDGFRβ and EGFR inhibition

(A) Effect of single therapy with lapatinib (100 mg/kg) on volume of tumor xenografts derived from PyMT+ cell lines from ambient air and physioxia (n = 4 to 5).

(B) Tumor volumes at 15th day of treatment with lapatinib. Graphs show higher T/C ratio in physioxia-derived xenografts compared to those derived from ambient air cells (n = 4 to 5).

(C) Combination of lapatinib (100 mg/kg) and sunitinib (20 mg/kg) shows synergistic growth inhibition in ambient air-derived tumor xenografts. There was no statistically significant difference in the tumor volumes of physioxia-derived tumor xenografts that were treated singly with sunitinib (20 mg/kg) and in combination (n = 4 to 5).

Figure 5. *Continued*

(D) Combination of lapatinib (100 mg/kg) and sunitinib (10 mg/kg) shows synergistic growth inhibition in physioxia-derived tumor xenografts. Tumor xenografts derived from cells grown in ambient air showed no response to treatment with sunitinib and the impact of lapatinib-sunitinib combination did not differ significantly from single treatment with lapatinib ($n = 5$).

(E) Effect of lapatinib and sunitinib on mediators of apoptosis, both singly and in combination in tumor tissues.

(F) Mouse body weights at beginning and end of 21-day treatment.

(G) Schematic representation of study findings (Created with BioRender.com). Tumor growth curves in A, C, and D were compared with two-way ANOVA, followed by Tukey's multiple comparisons test. Tumor growth rate in (B) was compared with a two-tailed Student's t test. Data are presented as means ± SD. *$p < 0.05$, **$p < 0.01$, ***$p < 0.001$, and ****$p < 0.0001$; ns, not significant. Western blot data are representative of 3 biologic replicates.

of both drugs in physioxia (Figure S5B). The expression of cleaved caspase-3 was, however, higher following concurrent treatment with both drugs (Figure S5B). The PyMT+ tumor cells in ambient air on the other hand did not show any meaningful changes in the expression of Mcl-1, Bcl-2, and Bcl-x but showed a decline in the expression of claspin and increased cleaved caspase-3 levels following combined treatment with lapatinib and sunitinib (Figure S5B). The apoptosis array showed no expression of HIF-1α in both physioxia and ambient air, suggesting no impact of HIF-1α signaling in the observed changes (Figure S5B). Western blotting of lysates derived from PyMT+ tumor cells treated concurrently with lapatinib and sunitinib in physioxia showed a decline in the expression of Mcl-1 and Bcl-2 but increased cleaved caspase-3 expression, independently confirming the aforementioned results (Figure 4G). The cells treated in ambient air showed a modest decrease in Mcl-1 expression and minimal expression of cleaved caspase-3 following drug combination (Figure 4G). In both ambient air and physioxia, the pro-apoptotic protein Bax showed no significant difference with single and combination treatment (Figure 4G).

Collectively, these data show that the differential O_2 tensions of ambient air and physioxia can significantly impact the kinome of cancer cells with consequent effects on how they respond to targeted drugs, particularly for combination therapies. Furthermore, our data suggest a significant role for apoptosis as the mechanism of cell death in the tumor cells treated with a combination of lapatinib and sunitinib particularly under physioxia.

Combination therapy with lapatinib and sunitinib induces dose-dependent synergistic growth inhibition *in vivo*

To determine if our *in vitro* observations hold true *in vivo*, we created tumor xenografts from PyMT+ tumor cells that were processed and propagated in ambient air and physioxia. The *in vivo* studies were carried out in two batches. In the first batch of experiments, we treated the tumor-bearing mice with lapatinib and sunitinib at respective doses of 100 mg/kg/day and 20 mg/kg/day both singly and in combination, with additional groups receiving vehicle control. Treatment was started when the tumors reached a volume of 100–150 mm^3 and continued for a duration of 15 days. Importantly, we have shown previously that tumors derived from the cells collected and processed in both ambient air and physioxia are histologically similar.[21] As observed in our previous work, the tumors formed from the PyMT+ cells grown in physioxia were less sensitive to single treatment with lapatinib, compared to the tumors formed from the ambient air cells (Figure 5A), as indicated by treatment-to-control ratios of 49.48% and 67.75% in the ambient air and physioxia cell-derived tumor xenografts, respectively, at the final day of treatment (Figure 5B). In this batch of *in vivo* studies, the effects of sunitinib on tumor growth in the physioxia cell-derived xenografts were relatively pronounced, compared to the tumors derived from the ambient air cells. For this reason, in contrast to the ambient air tumor cell xenografts, we did not observe synergistic growth inhibition of the lapatinib-sunitinib drug combination in the tumors formed from the physioxia cells (Figure 5C). Therefore, considering the efficacy of single treatment with sunitinib at 20 mg/kg/day, we repeated these studies using half the initial dose of sunitinib, with lapatinib maintained at the 100 mg/kg/day dose, this time, for a period of 21 days. In this series of experiments, we observed that the effects of single treatment with each drug and a combination of both drugs tracked more closely with what was observed *in vitro*. In the tumors derived from the cells grown in ambient air, single treatment with sunitinib had no significant impact on tumor growth (Figure 5D). In addition, there was no statistically significant difference in tumor growth inhibition induced by single treatment with lapatinib and a combination of lapatinib with sunitinib (Figure 5D). The tumors derived from the cells under physioxia, however, showed a different pattern of growth inhibition. We observed that there was no significant difference in tumor growth inhibition following single treatment with lapatinib or sunitinib (Figure 5D). However, a combination of lapatinib and sunitinib led to tumor growth inhibition that was significantly different from vehicle control and single treatment with lapatinib and sunitinib (Figure 5D). The observed reduction in efficacy of sunitinib alone suggests that while sunitinib may be effective on tumor cells with increased PDGFRβ activity, this effect is likely to be more significant at higher drug doses. To determine the potential role of apoptosis in tumor regression following drug combination, we evaluated the expression levels of the anti-apoptotic protein, Mcl-1, pro-apoptotic protein Bax, and cleaved caspase 3 in lysates prepared from residual tumors via western blotting. Surprisingly, we found that sunitinib enhanced the expression of Mcl-1 in ambient air and physioxia (Figure 5E). The stabilization of Mcl-1 was also observed with combination of lapatinib and sunitinib (Figure 5E). This finding is consistent with the previously reported dose-dependent stabilization of Mcl-1 by sunitinib.[51] However, Mcl-1 stabilization appeared to have no significant impact on apoptosis induction as the combination of lapatinib and sunitinib led to an increase in the expression of Bax and cleaved caspase-3 in the tumor tissues derived from PyMT+ cells under physioxia (Figure 5E). These findings indicate a role for apoptosis in tumor cell response to a combination of lapatinib and sunitinib, particularly under physioxia, albeit with unique dynamics in the expression or activity of apoptosis mediators *in vitro* and *in vivo*. Importantly, combined treatment with lapatinib and sunitinib was well tolerated by the mice, as there was no significant change in the mouse body weight across all the groups following the 21-day drug administration (Figure 5F). Altogether, these findings suggest an impact of the O_2 tension induced changes in tumor cell signaling on response to single treatment with targeted drugs as well as combination therapies.

DISCUSSION

O_2 levels in normal tissues are highly regulated and usually vary with the metabolic demands of each tissue type. Typically, levels are maintained between 3% and 9%.[10] Similarly, in solid tumors, O_2 levels vary depending on quality of blood supply and rate of O_2 consumption by the tumor cells with levels ranging from anoxic/hypoxic to physioxic from the core of the tumors to the periphery.[52] Regardless of a healthy or cancerous state, tumor O_2 levels are significantly lower than levels in ambient air. Despite this fact, routine approaches to preclinical cancer research often fail to consider the detrimental impact of ambient air on our understanding of cancer biology. Our experimental approach allows us to collect mouse mammary tumor and breast tissue from breast cancer-free human donors under physioxia such that exposure to ambient air is significantly minimized. We have previously demonstrated the effects of extraphysiologic O_2 shock/stress on tumor cell biology.[21] In this study, we have built upon our past work by further exploring signaling changes that occur due to physioxic and ambient O_2 tensions and how these changes contribute to tumor cell sensitivity or resistance to targeted drugs as well as combination therapies.

Our studies reveal a significant impact of the differential O_2 tensions on multiple kinases, notable among which include AKT and ERK. Activation of AKT and ERK in the tumor cells under physioxia correlates positively with the observed lack of sensitivity to treatment with BYL719 (alpelisib) and lapatinib, considering their protective roles against apoptotic cancer cell death and consequent contribution to drug resistance.[53] The activation of AKT and ERK under physioxia, however, appears to occur independent of EGFR signaling, since the level of activated EGFR was lower in physioxia. The lower level of active EGFR under physioxia may partially explain the observed lack of efficacy of EGFR inhibitors in tumors with EGFR protein overexpression, compared to those with EGFR activating mutations.[54,55] It is likely that the observed overexpression of EGFR is an artifact of prolonged exposure of the tumor tissues to ambient air prior to fixation. We found that the differential activation of AKT, and perhaps, ERK is likely to have occurred downstream of PDGFRβ activation under physioxia. Consistent with this finding, PDGFRβ has been reported to be a component of a feedback mechanism that activates AKT and ERK in both cancer and non-cancer cell lines.[40,56] Furthermore, phosphorylation of PDGFRβ on Y751 creates a binding site for P13K that subsequently activates AKT.[41,42] Our data suggest that the PDGFRβ-mediated activation of AKT and ERK under physioxia contributes to the reduced sensitivity of the tumor cells under physioxia to lapatinib. This possibility is supported by the observed efficacy of concurrent inhibition of EGFR and PDGFRβ in the cells under physioxia.

The expression of PDGFRβ is known to be associated with tumor stromal cells of mesenchymal origin, and its prognostic impact in breast cancer has also been reported.[57,58] Its expression in cells of epithelial origin is however not well elucidated. In this regard, basal-myoepithelial cells in mouse mammary gland have recently been shown to express PDGFRβ despite their epithelial phenotype.[44] Furthermore, higher expression of PDGFRβ has been associated with late-stage mammary tumors. Notably, Jechlinger and colleagues[38] reported the expression of PDGFRβ in late-stage, invasive breast intraductal carcinomas, compared to healthy breast tissue. In addition, a significant association between PDGFRβ expression and high tumor histologic grade has been reported.[59,60] The findings of this study reveal a previously unreported impact of O_2 tension on PDGFRβ expression. We demonstrated that the collection, processing, and culture of human breast epithelial cells and mouse tumor cells in physioxia not only activates PDGFRβ signaling but also affects the transcription and cell surface expression of the RTK. Although the observed lack of expression of the PDGF-BB ligand in the PyMT+ cells in ambient air and physioxia is consistent with findings of previous studies,[61] the reported absence of PDGFRβ expression in these cells could be attributed to the instability of the PDGFRβ protein in ambient air, as shown in this study. This warrants the need for further studies into the O_2-dependent impact of PDGFRβ on tumor biology, both *in vitro* and *in vivo*.

The data from this study suggest that in addition to PDGFRβ activation, the expression of the PDGFRβ mRNA and enrichment of PDGFRβ+ cells under physioxia may contribute, at least in part, to cancer cell stemness, tumor progression, and metastasis via epithelial-mesenchymal hybrid phenotype.[43] This notion is made evident by the enrichment of EMT-associated genes in PDGFRβ-expressing cells under physioxia despite a fraction of these cells maintaining epithelial characteristics. Indeed, the association between PDGFRβ activity and EMT has been demonstrated in cancer and non-malignant cells. For example, PDGFRβ was found to be expressed in immortalized human mammary epithelial cell lines in which EMT was induced via transduction of EMT-TFs.[62] Similarly, mesenchymal-like colorectal cell lines were observed to express PDGFRβ which promoted metastasis to the liver in experimental mouse models.[63] In addition, Shenoy and colleagues[64] described a role for PDGFRβ in cancer cells that underwent spontaneous or experimentally induced EMT, with a resulting acquisition of pericyte properties. Mechanistically, PDGFRβ activates protein kinase C alpha (PKCα), which in turn activates the EMT-TF, FOS-related antigen 1 that mediates the EMT phenotype and subsequent tumor progression.[49] This mechanism is also thought to mediate the generation of cancer stem cells, since cancer cells with "stem cell" traits can be generated as by-products of the EMT process.[49,65] We speculate that the EMT-associated mesenchymal state may have contributed to a switch from EGFR to PDGFRβ signaling as seen in the tumor cells under physioxia.[49] However, it is also possible that the switch to PDGFRβ signaling occurred prior to the adoption of the EMT-associated mesenchymal state.

Targeting PDGFRβ as a potential therapeutic approach for breast cancer has been geared mostly toward its impact on the development of the EMT state and subsequent metastasis or stem cell-mediated tumor progression. Notably, Thies et al.[61] reported the impact of paracrine PDGFB-PDGFRβ signaling between tumor stromal and epithelial cells on brain metastasis and demonstrated efficacy of the PDGFR inhibitor crenolanib on the mitigation of brain metastasis. Furthermore, based on the ability of the transcription factor forkhead box C2 (FOXC2) to mediate the expression of PDGFRβ in breast cancer cells induced to undergo EMT, prior studies have shown the capacity of the multikinase inhibitor sunitinib to inhibit tumor growth in FOXC2-expressing tumors.[66] In this study, we demonstrate a physioxia-dependent increase in PDGFRβ signaling in mammary tumor cells that leads to differential sensitivity to targeted therapies. Our data suggest that while PDGFRβ

expression can impact the development of an EMT state under physioxia, it is also capable of O_2-dependent signaling processes that can be targeted with combination therapy regimens. We demonstrate that the differential activity of PDGFRβ under physioxia renders tumor cells more susceptible to a combination of lapatinib and sunitinib both *in vitro* and *in vivo*, compared to those in ambient air. This suggests that the combination of lapatinib and sunitinib is a promising therapeutic approach, particularly in late-stage breast cancer. However, the efficacy of this drug combination is likely to be dependent on an increased expression/activity of PDGFRβ, in both tumor and stromal cells. In line with this, BRCA1-deficient tumors, which are characterized by increased PDGFRβ/PKCα signaling, are sensitive to PDGFRβ inhibition.[37] The observed lack of sensitivity of the tumor cells grown in ambient air to sunitinib, despite increased c-KIT (a known target of sunitinib) activity/expression, suggests a minimal biological impact of c-KIT expression in the tumor cells grown in ambient air, at least with respect to sensitivity to targeted therapies. This notion is supported by the likelihood of lower oncogenic implications of c-KIT in breast cancer, considering reported decreases in its expression with breast tissue malignancy.[35,67]

We observed decreased MIB binding of PI4K2A in the PyMT+ cells in ambient air compared to physioxia. However, studies on its biological impact are limited and are not fully understood. PI4K2A is involved in the synthesis of phosphatidylinositol 4-phosphate which is an essential substrate for the synthesis of phosphatidyl inositol (3, 4, 5)-trisphosphate and leads to the activation of AKT.[68] Furthermore, its role in the endosomal trafficking and degradation of activated EGFR has been elucidated.[69] Therefore, it is likely that the differential activation of PI4K2A in physioxia compared to ambient air leads to the regulation of AKT and EGFR activation in an opposing manner such that it facilitates the degradation of EGFR and the activation of AKT in physioxia-derived tumor cells. However, the role(s) of PI4K2A in the activation of AKT appears to be cell line dependent[70] and needs further studies, particularly in the context of physioxia.

The findings of this study have significant implications on current approaches to cancer biology research and development of treatment regimens. Our data show O_2-dependent differences in kinase signaling that impact sensitivity to targeted drugs (see schematic summary of findings in Figure 5G). This indicates that in continuous efforts to develop targeted therapies and combination therapy regimens, it may be necessary to consider the impact of physiologic O_2 tensions on potential drug targets. This could potentially paint a more reliable picture of the impact of candidate therapies on cancer biology and subsequently enhance the translation of preclinical cancer research.

Limitations of the study

The scRNA-seq analysis was performed using healthy breast epithelial cells, rather than breast carcinoma biopsies. While these samples enabled the identification of unique cell types expressing both epithelial and mesenchymal marker genes under physioxia, it does not necessarily explore gene expression patterns in the context of a tumor environment. Additional analyses involving human breast tumor tissues in ambient air and physioxia are being planned for future studies.

STAR★METHODS

Detailed methods are provided in the online version of this paper and include the following:

- KEY RESOURCES TABLE
- RESOURCE AVAILABILITY
  - Lead contact
  - Materials availability
  - Data and code availability
- EXPERIMENTAL MODEL AND STUDY PARTICIPANT DETAILS
  - Human subjects
  - Mouse models
- METHOD DETAILS
  - Tissue collection, processing and propagation of mammary tumor cells, primary breast epithelial cells, and human metastatic ovarian cancer cells
  - Single cell analysis of breast epithelial cells
  - Flow cytometry analysis and sorting
  - RNA isolation and quantitative reverse transcription polymerase chain reaction
  - *In vitro* and *in vivo* drug sensitivity and apoptosis assays
  - Multiplexed inhibitor beads (MIBs) kinome assay
  - Western blotting, receptor tyrosine kinase, apoptosis, and cytokine array
  - Transfections and gene knockdown
- QUANTIFICATION AND STATISTICAL ANALYSIS

SUPPLEMENTAL INFORMATION

Supplemental information can be found online at https://doi.org/10.1016/j.isci.2024.110068.

ACKNOWLEDGMENTS

These studies were performed in the Hypoxia Core at Indiana University School of Medicine, sponsored by the National Institutes of Health U54 DK106846. We acknowledge members of the Indiana University Simon Comprehensive Cancer Center (IUSCCC) flow cytometry core, medical genomics core, animal facility, and the Komen Tissue Bank at IUSCCC. We also thank the women who donated breast tissues for research and volunteers who enabled tissue collection.

This study was funded by Falk Medical Trust Catalyst and Transformative Award, Susan G Komen for the Cure, Komen ASPIRE Grant ASP231052685 (to H.N.), and IUSCCC Joe Ward Fellowship (to A.K.A.).

AUTHOR CONTRIBUTIONS

Conceptualization, A.K.A. and H.N.; methodology, A.K.A., P.B.-N., and H.N.; data acquisition, A.K.A., P.B.-N., C.D., S.P.A., C.E., H.G., N.G., B.K., Y.L., and H.N.; analysis and interpretation of data, A.K.A., C.D., S.P.A., C.E., H.G., N.G., and H.N.; administrative, technical, or material support, P.B.-N. and H.N.; writing, review and/or revision of manuscript, A.K.A. and H.N.; supervision, H.N.

DECLARATION OF INTERESTS

The authors declare no competing interests.

Received: December 15, 2023
Revised: April 5, 2024
Accepted: May 17, 2024
Published: May 21, 2024

REFERENCES

1. Siegel, R.L., Giaquinto, A.N., and Jemal, A. (2024). Cancer statistics, 2024. CA A Cancer J. Clin. *74*, 12–49. https://doi.org/10.3322/caac.21820.
2. Vasan, N., Baselga, J., and Hyman, D.M. (2019). A view on drug resistance in cancer. Nature *575*, 299–309. https://doi.org/10.1038/s41586-019-1730-1.
3. Boshuizen, J., and Peeper, D.S. (2020). Rational Cancer Treatment Combinations: An Urgent Clinical Need. Mol. Cell *78*, 1002–1018. https://doi.org/10.1016/j.molcel.2020.05.031.
4. Khatpe, A.S., Adebayo, A.K., Herodotou, C.A., Kumar, B., and Nakshatri, H. (2021). Nexus between PI3K/AKT and Estrogen Receptor Signaling in Breast Cancer. Cancers *13*, 369. https://doi.org/10.3390/cancers13030369.
5. An, J., Peng, C., Xie, X., and Peng, F. (2022). New Advances in Targeted Therapy of HER2-Negative Breast Cancer. Front. Oncol. *12*, 828438. https://doi.org/10.3389/fonc.2022.828438.
6. Konieczkowski, D.J., Johannessen, C.M., and Garraway, L.A. (2018). A Convergence-Based Framework for Cancer Drug Resistance. Cancer Cell *33*, 801–815. https://doi.org/10.1016/j.ccell.2018.03.025.
7. Yesilkanal, A.E., Johnson, G.L., Ramos, A.F., and Rosner, M.R. (2021). New strategies for targeting kinase networks in cancer. J. Biol. Chem. *297*, 101128. https://doi.org/10.1016/j.jbc.2021.101128.
8. Angus, S.P., Stuhlmiller, T.J., Mehta, G., Bevill, S.M., Goulet, D.R., Olivares-Quintero, J.F., East, M.P., Tanioka, M., Zawistowski, J.S., Singh, D., et al. (2021). FOXA1 and adaptive response determinants to HER2 targeted therapy in TBCRC 036. NPJ Breast Cancer *7*, 51. https://doi.org/10.1038/s41523-021-00258-0.
9. Aissa, A.F., Islam, A.B.M.M.K., Ariss, M.M., Go, C.C., Rader, A.E., Conrardy, R.D., Gajda, A.M., Rubio-Perez, C., Valyi-Nagy, K., Pasquinelli, M., et al. (2021). Single-cell transcriptional changes associated with drug tolerance and response to combination therapies in cancer. Nat. Commun. *12*, 1628. https://doi.org/10.1038/s41467-021-21884-z.
10. Adebayo, A.K., and Nakshatri, H. (2022). Modeling preclinical cancer studies under physioxia to enhance clinical translation. Cancer Res. *82*, 4313–4321. https://doi.org/10.1158/0008-5472.CAN-22-2311.
11. Jing, X., Yang, F., Shao, C., Wei, K., Xie, M., Shen, H., and Shu, Y. (2019). Role of hypoxia in cancer therapy by regulating the tumor microenvironment. Mol. Cancer *18*, 157. https://doi.org/10.1186/s12943-019-1089-9.
12. Bader, S.B., Dewhirst, M.W., and Hammond, E.M. (2020). Cyclic Hypoxia: An Update on Its Characteristics, Methods to Measure It and Biological Implications in Cancer. Cancers *13*, 23. https://doi.org/10.3390/cancers13010023.
13. Bertout, J.A., Patel, S.A., and Simon, M.C. (2008). The impact of O2 availability on human cancer. Nat. Rev. Cancer *8*, 967–975. https://doi.org/10.1038/nrc2540.
14. Muz, B., de la Puente, P., Azab, F., and Azab, A.K. (2015). The role of hypoxia in cancer progression, angiogenesis, metastasis, and resistance to therapy. Hypoxia *3*, 83–92. https://doi.org/10.2147/HP.S93413.
15. Batie, M., Frost, J., Frost, M., Wilson, J.W., Schofield, P., and Rocha, S. (2019). Hypoxia induces rapid changes to histone methylation and reprograms chromatin. Science *363*, 1222–1226. https://doi.org/10.1126/science.aau5870.
16. Chakraborty, A.A., Laukka, T., Myllykoski, M., Ringel, A.E., Booker, M.A., Tolstorukov, M.Y., Meng, Y.J., Meier, S.R., Jennings, R.B., Creech, A.L., et al. (2019). Histone demethylase KDM6A directly senses oxygen to control chromatin and cell fate. Science *363*, 1217–1222. https://doi.org/10.1126/science.aaw1026.
17. Mantel, C.R., O'Leary, H.A., Chitteti, B.R., Huang, X., Cooper, S., Hangoc, G., Brustovetsky, N., Srour, E.F., Lee, M.R., Messina-Graham, S., et al. (2015). Enhancing Hematopoietic Stem Cell Transplantation Efficacy by Mitigating Oxygen Shock. Cell *161*, 1553–1565. https://doi.org/10.1016/j.cell.2015.04.054.
18. Broxmeyer, H.E., O'Leary, H.A., Huang, X., and Mantel, C. (2015). The importance of hypoxia and extra physiologic oxygen shock/stress for collection and processing of stem and progenitor cells to understand true physiology/pathology of these cells ex vivo. Curr. Opin. Hematol. *22*, 273–278. https://doi.org/10.1097/MOH.0000000000000144.
19. Fogel, D.B. (2018). Factors associated with clinical trials that fail and opportunities for improving the likelihood of success: A review. Contemp. Clin. Trials Commun. *11*, 156–164. https://doi.org/10.1016/j.conctc.2018.08.001.
20. Sun, D., Gao, W., Hu, H., and Zhou, S. (2022). Why 90% of clinical drug development fails and how to improve it? Acta Pharm. Sin. B *12*, 3049–3062. https://doi.org/10.1016/j.apsb.2022.02.002.
21. Kumar, B., Adebayo, A.K., Prasad, M., Capitano, M.L., Wang, R., Bhat-Nakshatri, P., Anjanappa, M., Simpson, E., Chen, D., Liu, Y., et al. (2022). Tumor collection/processing under physioxia uncovers highly relevant signaling networks and drug sensitivity. Sci. Adv. *8*, eabh3375. https://doi.org/10.1126/sciadv.abh3375.
22. Christenson, J.L., Butterfield, K.T., Spoelstra, N.S., Norris, J.D., Josan, J.S., Pollock, J.A., McDonnell, D.P., Katzenellenbogen, B.S., Katzenellenbogen, J.A., and Richer, J.K. (2017). MMTV-PyMT and Derived Met-1 Mouse Mammary Tumor Cells as Models for Studying the Role of the Androgen Receptor in Triple-Negative Breast Cancer Progression. Horm. Cancer *8*, 69–77. https://doi.org/10.1007/s12672-017-0285-6.
23. Attalla, S., Taifour, T., Bui, T., and Muller, W. (2021). Insights from transgenic mouse models of PyMT-induced breast cancer: recapitulating human breast cancer

progression *in vivo*. Oncogene *40*, 475–491. https://doi.org/10.1038/s41388-020-01560-0.
24. Pfefferle, A.D., Herschkowitz, J.I., Usary, J., Harrell, J.C., Spike, B.T., Adams, J.R., Torres-Arzayus, M.I., Brown, M., Egan, S.E., Wahl, G.M., et al. (2013). Transcriptomic classification of genetically engineered mouse models of breast cancer identifies human subtype counterparts. Genome Biol. *14*, R125. https://doi.org/10.1186/gb-2013-14-11-r125.
25. Fry, E.A., Taneja, P., and Inoue, K. (2017). Oncogenic and tumor-suppressive mouse models for breast cancer engaging HER2/neu. Int. J. Cancer *140*, 495–503. https://doi.org/10.1002/ijc.30399.
26. Rojas, M., Yao, S., and Lin, Y.Z. (1996). Controlling epidermal growth factor (EGF)-stimulated Ras activation in intact cells by a cell-permeable peptide mimicking phosphorylated EGF receptor. J. Biol. Chem. *271*, 27456–27461. https://doi.org/10.1074/jbc.271.44.27456.
27. Alessi, D.R., Andjelkovic, M., Caudwell, B., Cron, P., Morrice, N., Cohen, P., and Hemmings, B.A. (1996). Mechanism of activation of protein kinase B by insulin and IGF-1. EMBO J. *15*, 6541–6551.
28. Hart, J.R., and Vogt, P.K. (2011). Phosphorylation of AKT: a mutational analysis. Oncotarget *2*, 467–476. https://doi.org/10.18632/oncotarget.293.
29. Chang, L., and Karin, M. (2001). Mammalian MAP kinase signalling cascades. Nature *410*, 37–40. https://doi.org/10.1038/35065000.
30. Zhang, D., Pal, A., Bornmann, W.G., Yamasaki, F., Esteva, F.J., Hortobagyi, G.N., Bartholomeusz, C., and Ueno, N.T. (2008). Activity of lapatinib is independent of EGFR expression level in HER2-overexpressing breast cancer cells. Mol. Cancer Therapeut. *7*, 1846–1850. https://doi.org/10.1158/1535-7163.MCT-08-0168.
31. Radu, M., and Chernoff, J. (2017). Recent advances in methods to assess the activity of the kinome. F1000Res. *6*, 1004. https://doi.org/10.12688/f1000research.10962.1.
32. Duncan, J.S., Whittle, M.C., Nakamura, K., Abell, A.N., Midland, A.A., Zawistowski, J.S., Johnson, N.L., Granger, D.A., Jordan, N.V., Darr, D.B., et al. (2012). Dynamic reprogramming of the kinome in response to targeted MEK inhibition in triple-negative breast cancer. Cell *149*, 307–321. https://doi.org/10.1016/j.cell.2012.02.053.
33. Sheikh, E., Tran, T., Vranic, S., Levy, A., and Bonfil, R.D. (2022). Role and significance of c-KIT receptor tyrosine kinase in cancer: A review. Bosn. J. Basic Med. Sci. *22*, 683–698. https://doi.org/10.17305/bjbms.2021.7399.
34. Abbaspour Babaei, M., Kamalidehghan, B., Saleem, M., Huri, H.Z., and Ahmadipour, F. (2016). Receptor tyrosine kinase (c-Kit) inhibitors: a potential therapeutic target in cancer cells. Drug Des. Dev. Ther. *10*, 2443–2459. https://doi.org/10.2147/DDDT.S89114.
35. Janostiak, R., Vyas, M., Cicek, A.F., Wajapeyee, N., and Harigopal, M. (2018). Loss of c-KIT expression in breast cancer correlates with malignant transformation of breast epithelium and is mediated by KIT gene promoter DNA hypermethylation. Exp. Mol. Pathol. *105*, 41–49. https://doi.org/10.1016/j.yexmp.2018.05.011.
36. Östman, A. (2017). PDGF receptors in tumor stroma: Biological effects and associations with prognosis and response to treatment. Adv. Drug Deliv. Rev. *121*, 117–123. https://doi.org/10.1016/j.addr.2017.09.022.
37. Bai, F., Liu, S., Liu, X., Hollern, D.P., Scott, A., Wang, C., Zhang, L., Fan, C., Fu, L., Perou, C.M., et al. (2021). PDGFRβ is an essential therapeutic target for BRCA1-deficient mammary tumors. Breast Cancer Res. *23*, 10. https://doi.org/10.1186/s13058-021-01387-x.
38. Jechlinger, M., Sommer, A., Moriggl, R., Seither, P., Kraut, N., Capodiecci, P., Donovan, M., Cordon-Cardo, C., Beug, H., and Grünert, S. (2006). Autocrine PDGFR signaling promotes mammary cancer metastasis. J. Clin. Invest. *116*, 1561–1570. https://doi.org/10.1172/JCI24652.
39. Heldin, C.H., Ostman, A., and Rönnstrand, L. (1998). Signal transduction via platelet-derived growth factor receptors. Biochim. Biophys. Acta *1378*, F79–F113. https://doi.org/10.1016/s0304-419x(98)00015-8.
40. Li, Q.L., Gu, F.M., Wang, Z., Jiang, J.H., Yao, L.Q., Tan, C.J., Huang, X.Y., Ke, A.W., Dai, Z., Fan, J., and Zhou, J. (2012). Activation of PI3K/AKT and MAPK pathway through a PDGFRβ-dependent feedback loop is involved in rapamycin resistance in hepatocellular carcinoma. PLoS One *7*, e33379. https://doi.org/10.1371/journal.pone.0033379.
41. Kazlauskas, A., and Cooper, J.A. (1990). Phosphorylation of the PDGF receptor beta subunit creates a tight binding site for phosphatidylinositol 3 kinase. EMBO J. *9*, 3279–3286. https://doi.org/10.1002/j.1460-2075.1990.tb07527.x.
42. Franke, T.F., Yang, S.I., Chan, T.O., Datta, K., Kazlauskas, A., Morrison, D.K., Kaplan, D.R., and Tsichlis, P.N. (1995). The protein kinase encoded by the Akt proto-oncogene is a target of the PDGF-activated phosphatidylinositol 3-kinase. Cell *81*, 727–736. https://doi.org/10.1016/0092-8674(95)90534-0.
43. Brabletz, S., Schuhwerk, H., Brabletz, T., and Stemmler, M.P. (2021). Dynamic EMT: a multi-tool for tumor progression. EMBO J. *40*, e108647. https://doi.org/10.15252/embj.2021108647.
44. Gray, G.K., Girnius, N., Kuiken, H.J., Henstridge, A.Z., and Brugge, J.S. (2023). Single-cell and spatial analyses reveal a tradeoff between murine mammary proliferation and lineage programs associated with endocrine cues. Cell Rep. *42*, 113293. https://doi.org/10.1016/j.celrep.2023.113293.
45. Yeeravalli, R., Kaushik, K., and Das, A. (2021). TWIST1-mediated transcriptional activation of PDGFRβ in breast cancer stem cells promotes tumorigenesis and metastasis. Biochim. Biophys. Acta, Mol. Basis Dis. *1867*, 166141. https://doi.org/10.1016/j.bbadis.2021.166141.
46. Szabo, P.M., Vajdi, A., Kumar, N., Tolstorukov, M.Y., Chen, B.J., Edwards, R., Ligon, K.L., Chasalow, S.D., Chow, K.H., Shetty, A., et al. (2023). Cancer-associated fibroblasts are the main contributors to epithelial-to-mesenchymal signatures in the tumor microenvironment. Sci. Rep. *13*, 3051. https://doi.org/10.1038/s41598-023-28480-9.
47. Roberts, W.G., Whalen, P.M., Soderstrom, E., Moraski, G., Lyssikatos, J.P., Wang, H.F., Cooper, B., Baker, D.A., Savage, D., Dalvie, D., et al. (2005). Antiangiogenic and antitumor activity of a selective PDGFR tyrosine kinase inhibitor, CP-673,451. Cancer Res. *65*, 957–966.
48. Atkins, M., Jones, C.A., and Kirkpatrick, P. (2006). Sunitinib maleate. Nat. Rev. Drug Discov. *5*, 279–280. https://doi.org/10.1038/nrd2012.
49. Tam, W.L., Lu, H., Buikhuisen, J., Soh, B.S., Lim, E., Reinhardt, F., Wu, Z.J., Krall, J.A., Bierie, B., Guo, W., et al. (2013). Protein kinase C alpha is a central signaling node and therapeutic target for breast cancer stem cells. Cancer Cell *24*, 347–364. https://doi.org/10.1016/j.ccr.2013.08.005.
50. Zheng, S., Wang, W., Aldahdooh, J., Malyutina, A., Shadbahr, T., Tanoli, Z., Pessia, A., and Tang, J. (2022). SynergyFinder Plus: Toward Better Interpretation and Annotation of Drug Combination Screening Datasets. Dev. Reprod. Biol. *20*, 587–596. https://doi.org/10.1016/j.gpb.2022.01.004.
51. Elgendy, M., Abdel-Aziz, A.K., Renne, S.L., Bornaghi, V., Procopio, G., Colecchia, M., Kanesvaran, R., Toh, C.K., Bossi, D., Pallavicini, I., et al. (2017). Dual modulation of MCL-1 and mTOR determines the response to sunitinib. J. Clin. Invest. *127*, 153–168. https://doi.org/10.1172/JCI84386.
52. Rakotomalala, A., Escande, A., Furlan, A., Meignan, S., and Lartigau, E. (2021). Hypoxia in Solid Tumors: How Low Oxygenation Impacts the "Six Rs" of Radiotherapy. Front. Endocrinol. *12*, 742215. https://doi.org/10.3389/fendo.2021.742215.
53. McCubrey, J.A., Steelman, L.S., Abrams, S.L., Lee, J.T., Chang, F., Bertrand, F.E., Navolanic, P.M., Terrian, D.M., Franklin, R.A., D'Assoro, A.B., et al. (2006). Roles of the RAF/MEK/ERK and PI3K/PTEN/AKT pathways in malignant transformation and drug resistance. Adv. Enzym. Regul. *46*, 249–279. https://doi.org/10.1016/j.advenzreg.2006.01.004.
54. Ali, R., and Wendt, M.K. (2017). The paradoxical functions of EGFR during breast cancer progression. Signal Transduct. Targeted Ther. *2*, 16042. https://doi.org/10.1038/sigtrans.2016.42.
55. Masuda, H., Zhang, D., Bartholomeusz, C., Doihara, H., Hortobagyi, G.N., and Ueno, N.T. (2012). Role of epidermal growth factor receptor in breast cancer. Breast Cancer Res. Treat. *136*, 331–345. https://doi.org/10.1007/s10549-012-2289-9.
56. Zhang, H., Bajraszewski, N., Wu, E., Wang, H., Moseman, A.P., Dabora, S.L., Griffin, J.D., and Kwiatkowski, D.J. (2007). PDGFRs are critical for PI3K/Akt activation and negatively regulated by mTOR. J. Clin. Invest. *117*, 730–738. https://doi.org/10.1172/JCI28984.
57. Prakash, J. (2016). Cancer-Associated Fibroblasts: Perspectives in Cancer Therapy. Trends Cancer *2*, 277–279. https://doi.org/10.1016/j.trecan.2016.04.005.
58. Strell, C., Stenmark Tullberg, A., Jetne Edelmann, R., Akslen, L.A., Malmström, P., Fernö, M., Holmberg, E., Östman, A., and Karlsson, P. (2021). Prognostic and predictive impact of stroma cells defined by PDGFRb expression in early breast cancer: results from the randomized SweBCG91RT trial. Breast Cancer Res. Treat. *187*, 45–55. https://doi.org/10.1007/s10549-021-06136-4.
59. D'Ippolito, E., Plantamura, I., Bongiovanni, L., Casalini, P., Baroni, S., Piovan, C., Orlandi, R., Gualeni, A.V., Gloghini, A., Rossini, A., et al. (2016). miR-9 and miR-200 Regulate PDGFRβ-Mediated Endothelial Differentiation of Tumor Cells in Triple-Negative Breast Cancer. Cancer Res. *76*, 5562–5572. https://doi.org/10.1158/0008-5472.CAN-16-0140.
60. Forte, L., Turdo, F., Ghirelli, C., Aiello, P., Casalini, P., Iorio, M.V., D'Ippolito, E., Gasparini, P., Agresti, R., Belmonte, B., et al.

(2018). The PDGFRβ/ERK1/2 pathway regulates CDCP1 expression in triple-negative breast cancer. BMC Cancer *18*, 586. https://doi.org/10.1186/s12885-018-4500-9.

61. Thies, K.A., Hammer, A.M., Hildreth, B.E., 3rd, Steck, S.A., Spehar, J.M., Kladney, R.D., Geisler, J.A., Das, M., Russell, L.O., Bey, J.F., 4th, et al. (2021). Stromal Platelet-Derived Growth Factor Receptor-beta Signaling Promotes Breast Cancer Metastasis in the Brain. Cancer Res. *81*, 606–618. https://doi.org/10.1158/0008-5472.CAN-19-3731.
62. Battula, V.L., Evans, K.W., Hollier, B.G., Shi, Y., Marini, F.C., Ayyanan, A., Wang, R.Y., Brisken, C., Guerra, R., Andreeff, M., and Mani, S.A. (2010). Epithelial-mesenchymal transition-derived cells exhibit multilineage differentiation potential similar to mesenchymal stem cells. Stem Cell. *28*, 1435–1445. https://doi.org/10.1002/stem.467.
63. Steller, E.J.A., Raats, D.A., Koster, J., Rutten, B., Govaert, K.M., Emmink, B.L., Snoeren, N., van Hooff, S.R., Holstege, F.C.P., Maas, C., et al. (2013). PDGFRB promotes liver metastasis formation of mesenchymal-like colorectal tumor cells. Neoplasia *15*, 204–217. https://doi.org/10.1593/neo.121726.
64. Shenoy, A.K., Jin, Y., Luo, H., Tang, M., Pampo, C., Shao, R., Siemann, D.W., Wu, L., Heldermon, C.D., Law, B.K., et al. (2016). Epithelial-to-mesenchymal transition confers pericyte properties on cancer cells. J. Clin. Invest. *126*, 4174–4186. https://doi.org/10.1172/JCI86623.
65. Luo, M., Brooks, M., and Wicha, M.S. (2015). Epithelial-mesenchymal plasticity of breast cancer stem cells: implications for metastasis and therapeutic resistance. Curr. Pharmaceut. Des. *21*, 1301–1310. https://doi.org/10.2174/1381612821666141211120604.
66. Hollier, B.G., Tinnirello, A.A., Werden, S.J., Evans, K.W., Taube, J.H., Sarkar, T.R., Sphyris, N., Shariati, M., Kumar, S.V., Battula, V.L., et al. (2013). FOXC2 expression links epithelial-mesenchymal transition and stem cell properties in breast cancer. Cancer Res. *73*, 1981–1992. https://doi.org/10.1158/0008-5472.CAN-12-2962.
67. Ko, C.D., Kim, J.S., Ko, B.G., Son, B.H., Kang, H.J., Yoon, H.S., Cho, E.Y., Gong, G., and Ahn, S.H. (2003). The meaning of the c-kit proto-oncogene product in malignant transformation in human mammary epithelium. Clin. Exp. Metastasis *20*, 593–597. https://doi.org/10.1023/a:1027323210736.
68. Waugh, M.G. (2012). Phosphatidylinositol 4-kinases, phosphatidylinositol 4-phosphate and cancer. Cancer Lett. *325*, 125–131. https://doi.org/10.1016/j.canlet.2012.06.009.
69. Minogue, S., Waugh, M.G., De Matteis, M.A., Stephens, D.J., Berditchevski, F., and Hsuan, J.J. (2006). Phosphatidylinositol 4-kinase is required for endosomal trafficking and degradation of the EGF receptor. J. Cell Sci. *119*, 571–581. https://doi.org/10.1242/jcs.02752.
70. Chu, K.M.E., Minogue, S., Hsuan, J.J., and Waugh, M.G. (2010). Differential effects of the phosphatidylinositol 4-kinases, PI4KIIα and PI4KIIIβ, on Akt activation and apoptosis. Cell Death Dis. *1*, e106. https://doi.org/10.1038/cddis.2010.84.
71. Butler, A., Hoffman, P., Smibert, P., Papalexi, E., and Satija, R. (2018). Integrating single-cell transcriptomic data across different conditions, technologies, and species. Nat. Biotechnol. *36*, 411–420. https://doi.org/10.1038/nbt.4096.
72. Stuart, T., Butler, A., Hoffman, P., Hafemeister, C., Papalexi, E., Mauck, W.M., 3rd, Hao, Y., Stoeckius, M., Smibert, P., and Satija, R. (2019). Comprehensive Integration of Single-Cell Data. Cell *177*, 1888–1902.e21. https://doi.org/10.1016/j.cell.2019.05.031.
73. Wickham, H. (2016). ggplot2: Elegant Graphics for Data Analysis (Springer-Verlag).
74. Prasad, M., Kumar, B., Bhat-Nakshatri, P., Anjanappa, M., Sandusky, G., Miller, K.D., Storniolo, A.M., and Nakshatri, H. (2019). Dual TGFβ/BMP Pathway Inhibition Enables Expansion and Characterization of Multiple Epithelial Cell Types of the Normal and Cancerous Breast. Mol. Cancer Res. *17*, 1556–1570. https://doi.org/10.1158/1541-7786.MCR-19-0165.
75. Bhat-Nakshatri, P., Gao, H., Sheng, L., McGuire, P.C., Xuei, X., Wan, J., Liu, Y., Althouse, S.K., Colter, A., Sandusky, G., et al. (2021). A single-cell atlas of the healthy breast tissues reveals clinically relevant clusters of breast epithelial cells. Cell Rep. Med. *2*, 100219. https://doi.org/10.1016/j.xcrm.2021.100219.
76. McCarthy, D.J., Campbell, K.R., Lun, A.T.L., and Wills, Q.F. (2017). Scater: pre-processing, quality control, normalization and visualization of single-cell RNA-seq data in R. Bioinformatics *33*, 1179–1186. https://doi.org/10.1093/bioinformatics/btw777.
77. Deane, F.M., Lin, A.J.S., Hains, P.G., Pilgrim, S.L., Robinson, P.J., and McCluskey, A. (2017). FD5180, a Novel Protein Kinase Affinity Probe, and the Effect of Bead Loading on Protein Kinase Identification. ACS Omega *2*, 3828–3838. https://doi.org/10.1021/acsomega.7b00020.
78. Daub, H., Olsen, J.V., Bairlein, M., Gnad, F., Oppermann, F.S., Körner, R., Greff, Z., Kéri, G., Stemmann, O., and Mann, M. (2008). Kinase-selective enrichment enables quantitative phosphoproteomics of the kinome across the cell cycle. Mol. Cell *31*, 438–448. https://doi.org/10.1016/j.molcel.2008.07.007.
79. Bantscheff, M., Eberhard, D., Abraham, Y., Bastuck, S., Boesche, M., Hobson, S., Mathieson, T., Perrin, J., Raida, M., Rau, C., et al. (2007). Quantitative chemical proteomics reveals mechanisms of action of clinical ABL kinase inhibitors. Nat. Biotechnol. *25*, 1035–1044. https://doi.org/10.1038/nbt1328.
80. Fisher, M.J., Shih, C.S., Rhodes, S.D., Armstrong, A.E., Wolters, P.L., Dombi, E., Zhang, C., Angus, S.P., Johnson, G.L., Packer, R.J., et al. (2021). Cabozantinib for neurofibromatosis type 1-related plexiform neurofibromas: a phase 2 trial. Nat. Med. *27*, 165–173. https://doi.org/10.1038/s41591-020-01193-6.
81. Perez-Riverol, Y., Bai, J., Bandla, C., García-Seisdedos, D., Hewapathirana, S., Kamatchinathan, S., Kundu, D.J., Prakash, A., Frericks-Zipper, A., et al. (2022). The PRIDE database resources in 2022: a hub for mass spectrometry-based proteomics evidences. Nucleic Acids Res. *50*, D543–D552. https://doi.org/10.1093/nar/gkab1038.

STAR★METHODS

KEY RESOURCES TABLE

REAGENT or RESOURCE	SOURCE	IDENTIFIER
Antibodies		
APC anti-mouse EpCAM	ThermoFisher Scientific	Cat# 17-5791-82; RRID:AB_2716944
PE anti-mouse CD140b (PDGFRbeta)	BioLegend	Cat# 136006; RRID:AB_1953271
APC isotype control antibody	BioLegend	Cat# 400612; RRID:AB_326556
PE isotype control antibody	BD Biosciences	Cat# 554689; RRID:AB_479724
Rabbit monoclonal anti-AKT (pan)	Cell Signaling Technology	Cat# 4691; RRID:AB_915783
Rabbit monoclonal anti-phospho-AKT (S473)	Cell Signaling Technology	Cat# 4060; RRID:AB_2315049
Rabbit monoclonal anti-α-tubulin	Cell Signaling Technology	Cat# 2144; RRID:AB_2210548
Rabbit monoclonal anti-phospho-EGFR (Y1068)	Cell Signaling Technology	Cat# 2234; RRID:AB_331701
Rabbit monoclonal anti-EGFR	Cell Signaling Technology	Cat# 4267; RRID:AB_2246311
Rabbit monoclonal anti-phospho-p44/42 MAPK (T202/Y204)	Cell Signaling Technology	Cat# 9101; RRID:AB_331646
Rabbit monoclonal anti-p44/42 MAPK	Cell Signaling Technology	Cat# 4695; RRID:AB_390779
Rabbit monoclonal anti-phospho-c-Kit (Y719)	Cell Signaling Technology	Cat# 3391; RRID:AB_2131153
Rabbit monoclonal anti-c-Kit	Cell Signaling Technology	Cat# 3074; RRID:AB_1147633
Rabbit monoclonal anti-phospho-PDGFRB (Y751)	Cell Signaling Technology	Cat# 3161; RRID:AB_331053
Rabbit monoclonal anti-PDGFRB	Cell Signaling Technology	Cat# 3169; RRID:AB_2162497
Rabbit monoclonal anti-Bcl-2	Cell Signaling Technology	Cat# 3498; RRID:AB_1903907
Rabbit monoclonal anti-Bax	Cell Signaling Technology	Cat# 2772; RRID:AB_10695870
Rabbit monoclonal anti-cleaved caspase 3	Cell Signaling Technology	Cat# 9661; RRID:AB_2341188
Mouse monoclonal anti-β-actin	Sigma-Aldrich	Cat# A5441; RRID:AB_476744
Anti-mouse IgG, HRP-linked Antibody	Cell Signaling Technology	Cat# 7076; RRID:AB_330924
Anti-rabbit IgG, HRP-linked Antibody	Cell Signaling Technology	Cat# 7074; RRID:AB_2099233
Biological samples		
Normal human breast tissue samples	Susan G. Komen Tissue Bank – IU Simon Comprehensive Cancer Center	N/A
Chemicals, peptides, and recombinant proteins		
Gentle Collagenase/Hyaluronidase	STEMCELL Technologies	Cat# 07919
Red blood cell lysis solution (10X)	Miltenyi Biotec	Cat# 130094183
Insulin	Sigma-Aldrich	Cat# I6634
Hydrocortisone	Sigma-Aldrich	Cat# H0888
Epidermal Growth Factor (EGF), human recombinant	Sigma-Aldrich	Cat# 01-107
Adenine	Sigma-Aldrich	Cat# A8626
ROCK inhibitor (Y-27632 hydrochloride)	Tocris Bioscience	Cat# A1254
BMP inhibitor (DMH-1)	Tocris Bioscience	Cat# A4126
TGFβ inhibitor (A 83-01)	Tocris Bioscience	Cat# A2939
Alpelisib (BYL719)	Selleckchem	Cat# S2814
Lapatinib	Selleckchem	Cat# S2111
Suntitinib malate	Selleckchem	Cat# S1042
Cycloheximide	Selleckchem	Cat# S7418
Polyethylene Glycol 300 (PEG300)	Selleckchem	Cat# S6704

(*Continued on next page*)

Continued

REAGENT or RESOURCE	SOURCE	IDENTIFIER
Tween 80	Selleckchem	Cat# S6702
cOmplete™ Protease Inhibitor Cocktail (Roche)	Millipore Sigma	Cat# 11697498001
Phosphatase Inhibitor Cocktail 2	Sigma-Aldrich	Cat# P5726
Phosphatase Inhibitor Cocktail 3	Sigma-Aldrich	Cat# P0044
Bio-Rad Protein Assay Dye Reagent Concentrate	Bio-Rad	Cat# 5000006
Critical commercial assays		
Chromium single cell 3′ reagents	10X Genomics	CG000183 Rev C
Bioanalyzer HSDNA chips	Agilent Technologies	G2943CA
RNeasy plus mini kit	Qiagen	Cat# A741340
iScript cDNA synthesis kit	Bio-Rad	Cat# 1708891
TaqMan Universal PCR Master Mix	ThermoFisher Scientific	Cat# 4324018
BrdU cell proliferation assay	Sigma-Aldrich	Cat# QIA58
Caspase-3 Assay Kit	Abcam	Cat# ab39401
Proteome Profiler Mouse Phospho-RTK Array	R&D Systems	Cat# ARY014
Proteome Profiler Mouse XL Cytokine Array	R&D Systems	Cat# ARY028
Proteome Profiler Mouse Apoptosis Array	R&D Systems	Cat# ARY031
Deposited data		
Single cell RNA sequencing data from breast epithelial cells from breast cancer-free donors	This paper	GEO: GSE244662
Mass spectrometry proteomics data. Deposited to the ProteomeXchange Consortium via the PRIDE partner repository	This paper	PRIDE: PXD046005
Experimental models: Cell lines		
PyMT+ mouse mammary tumor cell lines	This paper	N/A
Her2/Neu+ mouse mammary tumor cell lines	This paper	N/A
Human metastatic ovarian cancer cell line from ascites fluid	Kumar et al.[21]	N/A
Human breast epithelial cell line	This paper	N/A
Experimental models: Organisms/strains		
MMTV-PyMT transgenic mice	The Jackson Laboratory; Bred in-house	JAX: 002374; RRID:IMSR_JAX:002374
MMTV-Her2/Neu transgenic mice	The Jackson Laboratory; Bred in-house	JAX: 002376; RRID:IMSR_JAX:002376
FVB/NJ mice	The Jackson Laboratory; Bred in-house	JAX: 001800; RRID:IMSR_JAX:001800
Oligonucleotides		
Actb TaqMan assay	ThermoFisher Scientific	Mm02619580_g1
Snail1 TaqMan assay	ThermoFisher Scientific	Mm00441533_g1
Twist1 TaqMan assay	ThermoFisher Scientific	Mm00442036_m1
Zeb1 TaqMan assay	ThermoFisher Scientific	Mm00432087_m1
EGFR TaqMan assay	ThermoFisher Scientific	Mm01187858_m1
Accell™ Non-targeting Control siRNA	Dharmacon	Cat# D-001910-01-20
Accell™ Mouse Pdgfrb siRNA #1	Dharmacon	Cat# A-048218-14-0020
Accell™ Mouse Pdgfrb siRNA #2	Dharmacon	Cat# A-048218-16-0020
Software and algorithms		
FlowJo Software	FlowJo	https://www.flowjo.com/
MaxQuant (version 1.6.11.0)	MaxQuant	https://www.maxquant.org/
Perseus software (version 1.6.10.50)	MaxQuant	https://maxquant.net/perseus/

(*Continued on next page*)

Continued

REAGENT or RESOURCE	SOURCE	IDENTIFIER
ImageJ software (version 1.54f)	NIH	https://imagej.net/software/fiji/
GraphPad Prism software (version 10.1.0)	GraphPad	https://www.graphpad.com/features
CellRanger 3.0.2	10x Genomics	https://support.10xgenomics.com
bcl2fastq	Illumina	(https://support.illumina.com/)
Seurat R package (version 2.3.1)	Butler et al.[71] Stuart et al.[72]	https://satijalab.org/seurat/
ggplot2	Wickham et al.[73]	https://ggplot2.tidyverse.org.
Other		
Dulbecco's Modified Eagle's Medium (DMEM)	Corning	Cat# 10-013-CV
MEM Non-essential Amino Acids	Corning	Cat# 25-025-CI
Fetal Bovine Serum (FBS)	Sigma-Aldrich	Cat# F6178
Penicillin-Streptomycin	Sigma-Aldrich	Cat# P4333
Dulbecco's Modified Eagle's Medium (DMEM; low glucose)	Gibco	Cat# 12320-032
Ham's F-12 Nutrient Mix	Gibco	Cat# 11765-054
Illumina NovaSeq 6000 system	Illumina	https://www.illumina.com/systems/sequencing-platforms/novaseq.html
BD LSRFortessa (X-20) flow cytometer	BD Biosciences	https://www.bdbiosciences.com/en-us/products/instruments/flow-cytometers/research-cell-analyzers/bd-lsrfortessa-x-20
BD FACSAria Fusion flow cytometer	BD Biosciences	https://www.bdbiosciences.com/en-us/products/instruments/flow-cytometers/research-cell-sorters/bd-facsaria-fusion
T100® thermal cycler	Bio-Rad	Cat# 1861096
Applied Biosystems StepOnePlus real-time PCR system	ThermoFisher Scientific	Cat# 4376600
EASY-nLC™ 1200 System	ThermoFisher Scientific	Cat# LC140
Orbitrap Exploris™ 480 Mass Spectrometer	ThermoFisher Scientific	Cat# BRE725539
CondoCell™ portable physioxic isolation box. Coupled with purge unit	The Baker Company	https://bakerco.com/product/condocell/
COY CleanSpot PCR/UV hypoxic glovebox. Coupled with oxygen controller and CO_2 background gas controller	Coy Lab Products	https://coylab.com/
Xvivo System® Model X3 hypoxia incubator and glovebox system	Biospherix	https://biospherix.com/xvivo-system-model-x3/
Nuaire US Autoflow CO2 Water-Jacketed Incubator (Model number: NU4950)	Nuaire Laboratory Equipment	https://www.nuaire.com/products/co2-incubators/

RESOURCE AVAILABILITY

Lead contact

Further information and requests for resources should be directed to and will be fulfilled by the lead contact, Harikrishna Nakshatri (hnakshat@iu.edu).

Materials availability

Detailed information has been provided in the key resources table. Materials reported in this article will be shared by the lead contact upon request.

Data and code availability

- Data related to manuscript are included in the main manuscript or supplementary files. Source file contains all raw data and unprocessed western blot images. Single cell RNA sequencing data of breast epithelial cells from clinically breast cancer-free donors grown in physioxia and ambient air have been submitted to NCBI with accession number GEO: GSE244662. MIB kinome assay mass spectrometry proteomics data have been deposited to the ProteomeXchange Consortium via the PRIDE partner repository with the dataset identifier PRIDE: PXD046005.
- This paper does not report original code.
- Further information and requests should be directed to and will be fulfilled by the lead contact, Harikrishna Nakshatri (hnakshat@iu.edu).

EXPERIMENTAL MODEL AND STUDY PARTICIPANT DETAILS

Human subjects

Breast tissue samples were obtained from two clinically healthy, breast cancer free women with informed consent through tissue donation events organized by the Komen Tissue Bank (KTB) at Indiana University Simon Comprehensive Cancer Center. Sample collection was done in accordance with the International Ethical Guidelines for Biomedical Research involving Human Subjects and was approved by the International Review Board of Indiana University. Sample #1 was derived from a 71 year old female donor of European ancestry and Sample #2 is from a 36 year old female donor of European ancestry.

Mouse models

MMTV-PyMT, MMTV-Her2/Neu and FVB/NJ mice were initially purchased from The Jackson Labs and subsequently expanded in an in-house breeding colony. The Animal Care and Veterinary Services staff at Indiana University School of Medicine performed animal husbandry. The mice were held in individual cages holding a maximum of 5 mice, kept on a 12-hour light-dark cycle and fed *ad libitum*. Animal use in this study was approved by the Indiana University Animal Care and Use Committee (protocol #21056) and all procedures were performed in accordance with the National Institutes of Health guidelines. Only tumor tissues from female mice were used in these studies. The male mice were used for breeding purposes.

METHOD DETAILS

Tissue collection, processing and propagation of mammary tumor cells, primary breast epithelial cells, and human metastatic ovarian cancer cells

The metastatic ovarian cancer cells used in this study were derived in our previous work.[21] Tissue collection, processing and cell propagation procedures were designed to ensure that only tissues or cells intended for study in ambient air were exposed to air. Samples intended for physioxic O_2 tensions were handled solely in O_2 controlled workstations and incubators for the entirety of the experiments. Experimental steps required to be done outside the workstation such as incubation of tumor tissues and centrifugation were performed using sealed air-tight tubes to prevent exposure to air. Prior to initiation of experiments, all the required materials, including culture media, buffer solutions, tubes and pipettes were acclimated to the respective O_2 tensions (3% O_2 and 21% O_2) for 24 hours. For most of the experiments described in this study, cells were freshly processed and used within the first three passages to ensure consistency. Specific details regarding oxygen-controlled instrumentation can be found in the key resources table.

Tumor tissues were harvested from MMTV-PyMT and MMTV-Her2/Neu mice at 3% O_2, mechanically dissociated with a scalpel and forceps into fragments <1 mm in size and split into two portions. Each portion was exposed to ambient (21%) and physioxic (3%) O_2 tensions for 1 hour. The exposed tissues were processed into single cells via enzymatic digestion using a 10% collagenase/hyaluronidase formulation in tissue culture media for 90 minutes at 37°C in sealed 50 ml tubes. The dissociated tissues were then sterile filtered with a 70 μm strainer, washed in tissue culture media to remove the residual enzyme mixture and centrifuged at 1000 rpms for 5 minutes. The cells were then cultured either in a regular CO_2 incubator (ambient air) or at 5% O_2 in a physioxia incubator using Dulbecco's Modified Eagle's Medium. The culture media was supplemented with MEM Non-essential Amino Acids, 10% fetal bovine serum and 1% penicillin and streptomycin. To analyze the dissociated cells directly, without expansion in culture, the tumor tissues were processed as described above. Red blood cells were lysed and removed with treatment with a red cell lysis solution, washed and prepared for downstream analyses as appropriate.

Breast tissues from clinically breast cancer-free women were collected via core needle biopsy and transferred immediately (less than 30 seconds) into a portable hypoxia equipment for transportation to an oxygen-controlled workstation (3% O_2). Tissues were transported in the portable chamber to the workstation within seven minutes. The harvested tissues were then minced into fragments <1 mm in size, separated into two portions, and processed as described for the mouse mammary tumor tissues. The dissociated breast epithelial cells were subsequently cultured in a regular CO_2 incubator or at 5% O_2 with primary cell culture media containing low glucose DMEM and F-12 culture medium (in a 1:3 ratio). The culture medium was supplemented with 5% fetal bovine serum, 5 μg/ml bovine insulin, 0.4 μg/ml hydrocortisone and 20 ng/ml EGF and penicillin-streptomycin. The cells were plated on 804G conditioned media – coated plates with primary cell culture medium, further supplemented with 0.17 M adenine, 5 μmol/L of ROCK inhibitor Y-27632, 1 μmol/L of BMP inhibitor, DMH-1 and 1 μmol/L of TGFβ inhibitor A-83-01.[74]

Single cell analysis of breast epithelial cells

Normal breast epithelial cells that were processed and cultivated in ambient air and physioxia were harvested via trypsinization. Cell viability was measured by trypan blue exclusion and single cell status was determined via phase contrast microscopy. The harvested cells were subjected to cDNA library generation using 10X Genomics V3 Chromium Single Cell 3' Reagents (CG000183 Rev C). cDNA was quantified using HSDNA Chips on the Bioanalyzer from Agilent technologies and amplified with Chromium Single cell Library kit V3. The generated cDNA libraries were then sequenced to a read depth of ~50,000 reads per cell, using the Illumina NovaSeq 6000 system. Subsequent analysis of scRNA-seq sequence data was done as previously described.[75] Briefly, the generated raw sequence data was processed with CellRanger 3.0.2 which used bcl2fastq to demultiplex the raw base sequence calls into sample specific FASTQ files. The RNA-seq aligner STAR was then used to align the FASTQ files to GRCh38 human reference genome. Aligned reads were linked to individual cells and expression levels of each gene were determined based on number of unique molecular indices (UMIs) detected in individual cells. The filtered gene-cell barcode matrices generated by CellRanger were further analyzed with the Seurat R package (version 2.3.1).[71,72] For quality control (QC), genes detected in less than 5 cells and cells expressing less than 200 genes were filtered out. The isOutlier function in the scater R package, in addition to visual inspection of distribution in gene number, UMIs and mitochondrial gene content were used to further exclude low-quality cells.[76] This allowed for removal of cells with extremely high or low gene number/UMIs and cells with high percentage of mitochondrial reads. Following removal of low-quality cells and potential doublets/multiplets, the NormalizeData function in Seurat was used to normalize gene expression levels in individual cells. Furthermore, the ScaleData function was used to linearly regress out variations from different numbers of UMIs and mitochondrial gene expression.

To integrate single cell data from samples of individual donors, the FindIntegrationAnchors and IntegrateData functions in Seurat v3 were used. This was followed by scaling and principal component analysis (PCA) of the integrated data. The Seurat functions FindNeighbors and FindClusters were then used to identify individual clusters. To identify cell types in each cluster, the FindConservedMarkers function was used to identify canonical type marker genes. Cell clusters were visualized by Uniform Manifold Approximation and Projection (UMAP) plots. The ggplot2 and FeaturePlot R packages were used to generate feature plots to visualize the expression patterns of specific genes across all clusters.[73]

Flow cytometry analysis and sorting

Adherent PyMT and Her2/Neu tumor cells were harvested via trypsinization and stained for flow cytometry using antibodies conjugated to fluorescent labels. The antibodies used against the PyMT and Her2 tumor cells were EpCAM–APC (allophycocyanin) and CD140b (PDGFRB)-PE (phycoerythrin). To determine abundance of PDGFRβ^+ cells in the tumors, PyMT+ and Her2/neu+ mammary tumors were processed into single cells as described above and stained without expansion in culture. The stained cells were acquired with BD LSRFortessa (X-20) flow cytometer and analyzed using the FlowJo software. To sort the Her2/Neu+ mouse tumor cell line, the harvested cells were stained with the EpCAM-APC and CD140b (PDGFRB)-PE antibodies and sorted with a BD FACSAria Fusion flow cytometer. Sorted cells were then expanded in physioxia for subsequent analysis via qRT-PCR.

RNA isolation and quantitative reverse transcription polymerase chain reaction

Total RNA was extracted from the tumor cells using the RNeasy kit under the respective O_2 tensions following manufacturer's instructions. 1 μg of the extracted RNA was used to synthesize complementary DNA (cDNA), using the iScript cDNA synthesis kit in a Bio-Rad T100® thermal cycler. The synthesized cDNA was then used to perform quantitative reverse transcription polymerase chain reaction (qRT-PCR) using TaqMan assay primers targeted to *Actb*, *Snai1*, *Twist1*, *Zeb1*, and *Egfr*. The qRT-PCR was performed with the TaqMan Universal PCR Master Mix, using an Applied Biosystems StepOnePlus real-time PCR system for fluorescence detection.

In vitro and *in vivo* drug sensitivity and apoptosis assays

For the *in vitro* drug sensitivity assays, 2 x 10^3 PyMT and Her2/Neu mouse tumor cell lines processed and propagated in ambient air and physioxia were seeded into 96-well plates and treated with indicated concentrations of BYL719 (alpelisib), lapatinib or sunitinib for 48 hours in the respective O_2 tensions. Prior to the end of treatment duration, the cells were labelled with bromodeoxyuridine (BrdU), fixed, and developed using a BrdU enzyme-linked immunosorbent assay (ELISA) kit and analyzed for proliferation rate following manufacturer's instructions. Apoptosis was assessed by analyzing caspase-3 activity, using a Caspase-3 Assay Kit following manufacturer's instructions.

To perform the *in vivo* drug sensitivity assays, PyMT+ mouse tumor cells (2 x 10^6, in 100 μl volume of PBS) cultured in ambient air and physioxia were injected into the fifth inguinal mammary fat pad of 6- to 7-week-old syngeneic FVB/N mice. To ensure that the tumor cells under physioxia were continually protected from exposure to air, the cells were aspirated into syringes previously acclimated to physioxia, sealed completely with needle and cap and kept on ice in an airtight container. Tumor sizes were measured using calipers and tumor volume (in cubic millimeters [mm^3]) was calculated using the formula: sagittal dimension (mm) x [cross dimension (mm)]^2/2. When the tumors reached average sizes of 100-150 mm^3 or 150-200 mm^3 in the first and second batch of experiments, respectively, the mice were randomized into the indicated groups and treatment was initiated. The mice were treated either with the vehicle control or targeted drugs lapatinib and sunitinib either singly or in combination. In both sets of *in vivo* studies, lapatinib was used at a dosage of 100 mg/kg body weight, while sunitinib was administered at a dosage of 20- and 10 mg/kg body weight in the first and second *in vivo* study sets, respectively. Both drugs were prepared in

polyethylene glycol 300 (PEG300), Tween 80 and water as per manufacturer's instructions. The vehicle control and drugs were administered daily via oral gavage for 15 and 21 days in the first and second study batches, respectively. Tumor growth was measured every 3 days.

Multiplexed inhibitor beads (MIBs) kinome assay

PyMT+ cells were treated with 1 μM lapatinib or DMSO for 48 hours in ambient air and physioxia and then lysed in MIBs lysis buffer (50 mM HEPES, 150 mM NaCl, 0.5% Triton X-100, 1 mM EDTA, 1 mM EGTA, pH 7.5) supplemented with complete protease inhibitor cocktail and 1% phosphatase inhibitor cocktails 2 and 3. Extracts were clarified by centrifugation, and protein concentration was quantified by the Bradford assay. Equal amounts of total protein were gravity-flowed over MIB columns in high-salt MIB lysis buffer (1 M NaCl). The MIB columns consisted of a 125-μl mixture of six type I kinase inhibitors: VI-16832, PP58, purvalanol B,[77] UNC-00064-12, UNC00064-79, and BKM-120, which were custom synthesized with hydrocarbon linkers and covalently linked to ECH-Sepharose.[32,78–80] Bound protein was eluted twice with 0.5% SDS, 1% β-mercaptoethanol, 100 mM Tris-HCl, pH 6.8 for 15 min at 100C, and then treated with dithiothreitol (5 mM) for 25 min at 60°C and 20 mM iodoacetamide for 30 min in the dark. Following concentration by centrifuging with Amicon Ultra-4 filters (10-kDa cutoff) to ~100 μl, samples were precipitated with methanol–chloroform, dried in a SpeedVac, and resuspended in 50 mM HEPES (pH 8.0). Tryptic digests were performed overnight at 37°C, extracted four times with 1 ml ethyl acetate to remove detergent, and dried, and peptides were passed through C18 spin columns according to the manufacturer's protocol (Pierce). Peptides were resuspended in 0.1% formic acid and equal volume (approximately 20% of the final peptide suspension for each experimental set) was injected onto a Thermo EASY-Spray 75 μm × 25 cm C18 column and separated on a 120-min gradient (2–40% acetonitrile) using an EASY-nLC 1200 instrument. The Thermo Orbitrap Exploris 480 MS ESI parameters were as follows: Full Scan – Resolution 120,000, Scan range 375-1500 m/z, RF Lens 40%, AGC Target - Custom (Normalized AGC Target, 300%), 60 sec maximum injection time, Filters – Monoisotopic peak determination: Peptide, Intensity Threshold 5.0e3, Charge State 2-5, Dynamic Exclusion 30 sec, Data Dependent Mode – 20 Dependent scans, ddMS2 – Isolation Window 2 m/z, HCD Collision Energy 30%, Resolution 30,000, AGC Target – Custom (100%), maximum injection time 60 sec. Raw files were processed for label-free quantification (LFQ) by MaxQuant LFQ using the UniProt/Swiss-Prot mouse database with fixed carbidomethyl (C) and variable oxidation (M) and acetyl (protein N-terminal) modifications, match time window 3 min. LFQ intensities for all annotated kinases with at least two razor+unique peptides were imported into Perseus software, log2 transformed, filtered to include annotated kinases with at least three valid values in one treatment group, and missing values imputed from the normal distribution for each column using default parameters (width 0.3, down shift 1.8). Two sample, unpaired Student t-tests of log2LFQ intensities were performed and plotted using R ($P<0.05$ significance cut-off). The mass spectrometry proteomics data have been deposited to the ProteomeXchange Consortium via the PRIDE partner repository (PXD046005).[81]

Western blotting, receptor tyrosine kinase, apoptosis, and cytokine array

Cell lysates from processed tumor or cultured cells were prepared by lysis in radioimmunoprecipitation assay (RIPA) buffer containing protease inhibitors. The Bradford assay was used for protein quantitation and 10 - 25 μg of extract was used for Western blotting. The cell lysates were resolved in 8% to 12% sodium dodecyl sulfate polyacrylamide gel electrophoresis (SDS-PAGE), followed by blotting onto a polyvinylidene difluoride (PVDF) membrane. The primary antibodies used in this study are rabbit anti-Akt (pan), rabbit anti-phospho-Akt (Ser473), rabbit anti-α-tubulin, rabbit anti-phospho-EGF receptor (Tyr1068), rabbit anti-EGF receptor, rabbit anti-phospho-p44/42 MAPK (Thr202/Tyr204), rabbit anti-p44/42 MAPK, rabbit anti-phospho-c-Kit (Tyr719), rabbit anti-c-Kit, rabbit anti-PDGF receptor β, rabbit anti-phospho-PDGF Receptor β (Tyr751), rabbit anti-Mcl-1, rabbit anti-Bcl-2, rabbit anti-Bax, rabbit anti-cleaved caspase-3, and mouse anti-β-actin. The protein bands were visualized via chemiluminescence detection.

RTK phosphorylation in cell lysates (200 μg protein) was evaluated with a mouse phospho-RTK array kit following manufacturer's instructions. For the cytokine array, serum free supernatants of PyMT+ tumor cells collected after overnight incubation in serum free media in ambient air and physioxia were screened for multiple cytokine levels using a mouse cytokine array kit following manufacturer's instructions. Analysis of the expression of apoptosis-related proteins in treated mammary tumor cells was done with a mouse apoptosis array kit following manufacturer's instructions. Quantification of western blot and apoptosis array data was performed using ImageJ software.

Unedited Western blot, RTK array, cytokine array and apoptosis array data are shown in Table S3.

Transfections and gene knockdown

PyMT+ and Her2/Neu+ mouse tumor cells (5×10^5) grown in physioxia and ambient air in 60 mm tissue culture dishes were transfected with two Accell™ mouse PDGFRβ siRNA constructs targeting the 3'UTR and a non-targeting control siRNA in serum-free media at a concentration of 1 μM, following manufacturer's instructions. Protein level was assayed via Western blotting 96 hours after transfection.

QUANTIFICATION AND STATISTICAL ANALYSIS

Two-tailed Student's t-test was performed on replicates to determine statistical significance between any two conditions. Analyses involving comparisons involving multiple groups were conducted using one- or two-way Analysis of Variance (ANOVA) and followed by the appropriate post-hoc tests. Statistical analyses were conducted using the GraphPad Prism software. Data are presented as mean ± SD. * $P < 0.05$, ** $P < 0.01$, *** $P < 0.001$, and **** $P < 0.0001$; ns, not significant. Additional statistical details can be found in the figure legends. Source data are available in Table S3.